Spatially continuous snow depth mapping by airplane photogrammetry for annual peak of winter from 2017 to 2021 in open areas

Leon J. Bührle[1,2], Mauro Marty[3], Lucie A. Eberhard[1,2,4], Andreas Stoffel[1,2], Elisabeth D. Hafner[1,2,5], Yves Bühler[1,2]

[1] WSL Institute for Snow and Avalanche Research SLF, Davos Dorf, 7260, Switzerland
[2] Climate Change, Extremes and Natural Hazards in Alpine Regions Research Center CERC, 7260 Davos Dorf, Switzerland
[3] Swiss Federal Institute for Forest, Snow and Landscape Research WSL, Birmensdorf, 8903, Switzerland
[4] Institute of Geodesy and Photogrammetry, ETH Zurich, Zurich, 8092, Switzerland
[5] EcoVision Lab, Photogrammetry and Remote Sensing, ETH Zurich, Zurich, 8092, Switzerland

Correspondence to: Yves Bühler (buehler@slf.ch)

Abstract.

Information on snow depth and its spatial distribution is important for numerous applications such as the assessment of natural hazards, the determination of the available snow water equivalent for hydropower, the dispersion and evolution of flora and fauna and the validation of snow-hydrological models. Due to the heterogeneity and complexity of snow depth distribution in alpine terrain, only specific remote sensing tools are able to accurately map the present variability. To cover large areas (>100 km²), airborne laser scanners (ALS) or survey cameras mounted on piloted aircrafts are needed. Applying the active ALS leads to considerably higher costs compared to photogrammetry but also works better in forested terrain. The passive photogrammetric method is more economic but limited due to its dependency on good acquisition conditions (weather, sufficient light). In this study, we demonstrate the reliable and accurate photogrammetric processing of high spatial resolution (0.5 m) annual snow depth maps during peak of winter over a 5-year period under different acquisition conditions within a study area around Davos, Switzerland. Compared to previously carried out studies, using the new Vexcel Ultracam Eagle M3 survey sensor improves the average ground sampling distance to 0.1 m at similar flight altitudes above ground. This allows for very detailed snow depth maps in open areas, calculated by subtracting a snow-free digital terrain model (DTM acquired with ALS) from the snow-on digital surface models (DSMs) processed from the airborne imagery. Despite complex acquisition conditions during the recording of the Ultracam images (clouds, shaded areas and new-snow cover), 99 % of unforested areas were successfully reconstructed. We applied masks (high vegetation, settlements, water, glaciers) to significantly increase the reliability of the snow depths measurements. An extensive accuracy assessment including the use of check points, the comparison to DSMs derived from unpiloted aerial systems, and the comparison of snow-free pixels to the ALS-DTM prove the high quality and accuracy of the generated snow depth maps. We achieve a root mean square error of approximately 0.25 m for the Ultracam X and 0.15 m for the successor sensor Ultracam Eagle M3. By developing an almost

consistent and reliable photogrammetric workflow for accurate snow depth distribution mapping over large regions, we provide a new tool for analysing snow distribution in complex terrain. This enables more detailed investigations on seasonal snow dynamics, can be used for numerous applications related to snow depth distribution as well as avalanches and serves as ground reference for new modelling approaches as well as satellite-based snow depth mapping.

1 Introduction

Accurate snow depth mapping is important for the assessment, prediction and prevention of natural hazards such as snow avalanches or floods. Crack propagation and the size of release areas of snow avalanches are, for example, linked to snow depth distribution (Veitinger und Sovilla 2016; Schweizer et al. 2003). The snow distribution, and therefore avalanches, are simultaneously influenced by wind induced snow-drift in the starting zone as well as the avalanche path (Schön et al. 2015). Further hazards related to snow depth are snow loads on buildings, threatening not only the stability of roofs but potentially leading to dangerous roof avalanches (Croce et al. 2018). Additionally, snow depth and the corresponding snow water equivalent (SWE) are crucial for flood forecasting. Various economic sectors can benefit from accurate snow depth information, for example, the available SWE is a key criterion for the implementation and operation of hydropower (Magnusson et al. 2020). Detailed information on snow depth distribution on slopes is also valuable for winter resorts (Spandre et al. 2017). Moreover, snow depth mapping facilitates research on interactions between snow depth distribution and flora as well as fauna (Wipf et al. 2009).

Precise snow depth measurements are key data when validating models for snow parameters. In avalanche modelling tools such as the Rapid Mass Movement Simulation (RAMMS) (Christen et al. 2010), the snow volume derived from snow depth maps can be compared to modelled results. Furthermore, snow depth maps can serve as reference for snow depth distribution models (Wulf et al. 2020) and snow-hydrological models like Alpine3D (Richter et al. 2021; Schlögl et al. 2018; Vögeli et al. 2016; Brauchli et al. 2017), Factorial snowpack model (FSM) (Essery 2015) and Crocus (Brun et al. 1992). From high spatial resolution snow depth maps, the fractional snow-covered area parameter can also be compiled (Helbig et al. 2021).

Traditionally, snow depth is measured by field observations such as manual probing or by automated weather stations (AWS). However, interpolation is required to get a spatially continuous coverage. As snow depths vary a lot over short distances, especially in complex terrain (Grünewald et al. 2010; Grünewald et al. 2014), interpolation is insufficient for most applications. Ground-penetrating radar (GPR) can capture many point measurements when mounted on a sledge or snowmobile (Helfricht et al. 2014) with a high accuracy of less than 0.1 m (Griessinger et al. 2018). Still, only transects and spatially non-continuous snow depth distribution are measured (McGrath et al. 2019).

Remote sensing tools can provide accurate and spatially continuous snow depth measurements. Terrestrial laser scanning (TLS), based on the reflectance of laser beams on object surfaces, can provide very exact measurements (Deems et al. 2013). The achieved accuracy depends on the sensor and the object's distance from the scanner and ranges from 0.05 m to 0.2 m in distances below 1000 m (Grünewald et al. 2010; Prokop 2008) and 0.3 m to 0.6 m over longer distances of around 3000 m (López-Moreno et al. 2017). Another crucial advantage is the lower weather-dependency regarding the illumination conditions. Limitations of this procedure are the access to locations for the scanner, the occurrence of concealed areas which cannot be measured and poor weather conditions such as strong snowfall (Prokop 2008).

In recent years, the use of digital photogrammetric methods has increased mainly due to the development of the SIFT-algorithm (Lowe 2004), easy to apply softwares like Agisoft Metashape or Pix4D and the development of unpiloted aerial systems (UAS). The accuracy of snow depths derived from UAS photogrammetry, which mainly depends on the sensor, the ground sampling distances (GSD) as well as collection conditions, ranging from 0.05 m to 0.2 m (Bühler et al. 2016; Michele et al. 2016; Harder et al. 2016). Critical issues for this method are the dependency on good weather and light conditions (Bühler et al. 2017; Gindraux et al. 2017) and the difficulties of measuring snow depths in areas with high vegetation. Unpiloted aerial laser scanning systems (ULS) combine the advantages of TLS and UAS and can measure snow depths with a high accuracy of around 0.1 m in unforested (Jacobs et al. 2021) and 0.2 m in forested terrain (Harder et al. 2020). However, the current UAS, ULS and TLS can only capture areas up to 5 km² (Revuelto et al. 2021).

To map larger regions, airborne laser scanners (ALS), airplane photogrammetry or satellites are needed. For satellites, both Pléiades and Worldview-3, offer high temporal resolution and trough (triple) stereo acquisitions allow for large-scale snow depth mapping (Marti et al. 2016). However, first studies have shown that snow depth measurements from Pléiades imagery in comparison to reference data exhibit a root mean square error (RMSE) of more than 0.5 m (Deschamps-Berger et al. 2020; Eberhard et al. 2021; Shaw et al. 2020). These accuracies do not satisfy the requirements for most snow depth mapping applications. The study of McGrath et al. (2019) applied the WorldView-3 satellite with a GSD of 0.3 m (resampled to 8 m grid) and achieved a considerably higher accuracy with a RMSE of 0.24 m compared to GPR.

In contrast to satellite measurements, ALS achieves accuracies similar to the one of TLS (Mazzotti et al. 2019; Deems et al. 2013). However, Bühler et al. (2015) estimated the cost for an ALS-flight and the processing of the data to be around 50'000 to 80'000 CHF, covering an area of 150 km². Current inquiries on different companies confirm these high costs, which prevent the realisation for many implementations. Airplane-based photogrammetry, however, is more economic with costs ranging from 30'000 to 60'000 CHF for the same area (Bühler et al. 2015). Despite the application of a lower cost camera (Nikon D800E), Nolan et al. (2015) successfully created snow depth maps over small areas (5 - 40 km²) and reached an excellent accuracy of about 0.1 to 0.2 m. Bühler et al. (2015) produced a high-resolution snow depth map with a spatial resolution of 2 m, covering a heterogeneous high-mountain area of 300 km² around Davos. Using the surveying pushbroom-scanner Leica

ADS 80, a RMSE of 0.3 m comparing to GPR, TLS and probing was achieved. Meyer et al. (2022) created a snow depth map with 1 m spatial resolution covering an area of 300 km² and demonstrated that airplane-based photogrammetry can reach accuracies similar to the ones of the ALS. The new state-of-the art 450 Megapixel (MP) frame sensor Vexcel Ultracam Eagle M3 can record extremely high spatial resolution images, which enables the generation of accurate large-scale digital surface models (DSM). Eberhard et al. (2021) achieved an accuracy of around 0.1 m using the Vexcel Ultracam Eagle M3 as well as 29 ground control points (GCPs) to refine the orientation within a small catchment (40 km²).

In this study, we present the consistent processing of five annual snow depth maps with a spatial resolution of 0.5 m based on Vexcel Ultracam images covering approximately 230 km² each year. These datasets were acquired at peak of winter, capturing large differences in average snow depths as well as various weather and illumination conditions were observed between the different years.

2 Study area Davos, Switzerland

The study area is located around Davos in Eastern Switzerland. A core area with an extent of approximately 230 km² was covered by all flight campaigns from 2019 to 2021. However, the total area acquired per year differs due to varying flight routes during image recording (Fig. 1). The elevation of the main study area ranges from 1100 m a.s.l around Klosters to the 3229 m a.s.l. high Piz Vadret. The diversity of the terrain, including extremely steep faces, large heterogeneous as well as open areas, settlements, forested and glaciated areas is representative for many mountain regions. The research area is located in a transition zone between the humid north-alpine climate and the drier climate zone of the central Alps (Kulakowski et al. 2011; Mietkiewicz et al. 2017). The main snowfall in the winter season is recorded during north-westerly and northern weather situations, which are commonly connected to strong storms with high wind speeds (Gerber et al. 2019; Mott et al. 2010).

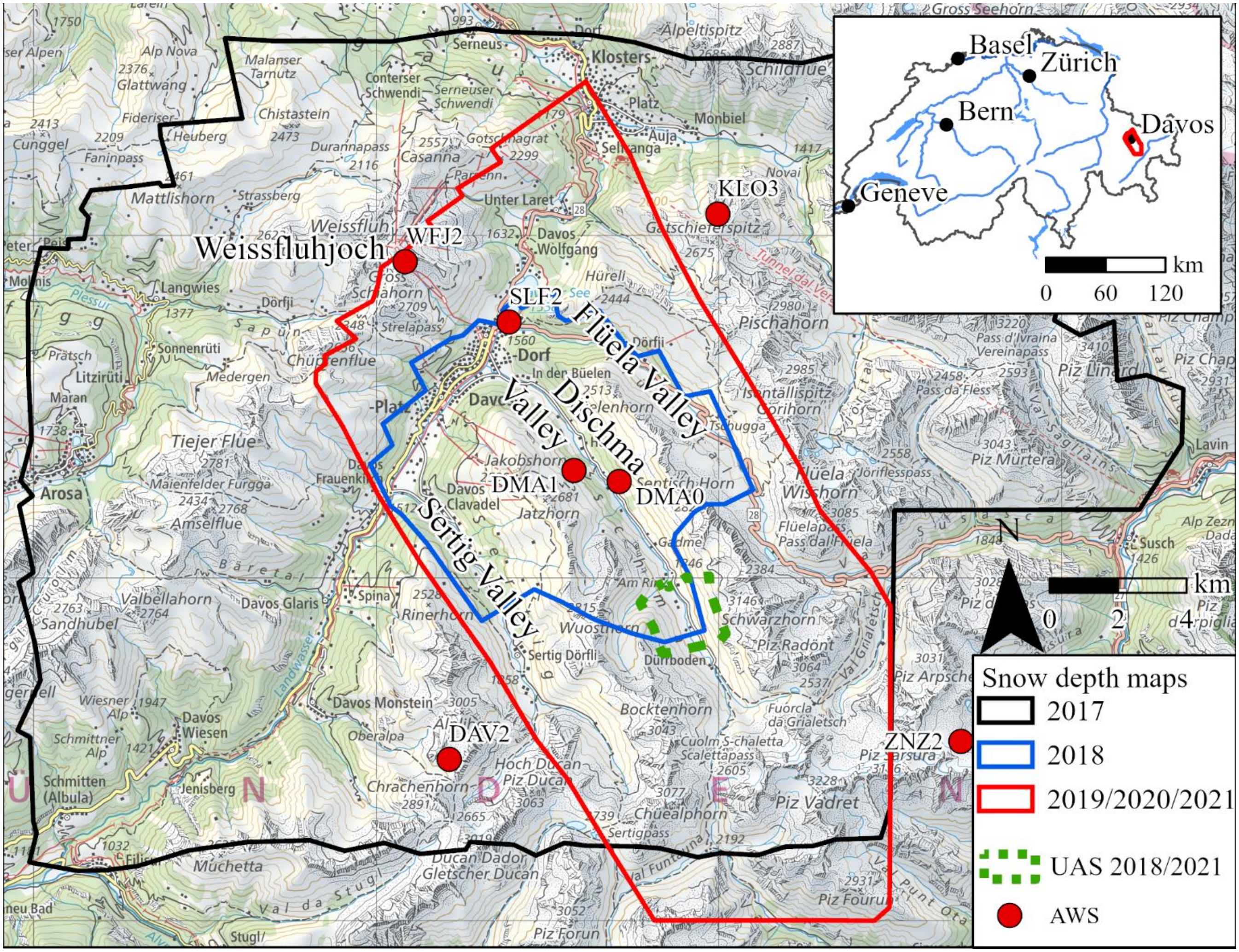

Figure 1. Overview of the study area: Snow depth map generated by the airplane 2017 (black), extent of snow depth map from 2018 (blue) and snow depth area derived from the respective flights in 2019, 2020 and 2021 (red; corresponds to main study area). Additionally, the area covered by the UAS for reference data in 2018 and 2021 are shown (green). The red points symbolise the location of the automatic weather stations with accurate snow depth measurements. The red polygon in the inset map depicts the location of the main study area in Switzerland (map source: Federal Office of Topography).

3 Data and sensor

3.1 Vexcel Ultracam

Airborne imagery was acquired with the survey camera Vexcel Ultracam series. The Vexcel Ultracam X was applied in 2017, and is characterised by a sensor pixel size of 7.2 µm x 7.2 µm, a focal length of 100.5 mm and a resolution of 14430 x 9420 pixels (Schneider und Gruber 2008). Due to better characteristics of the camera Ultracam Eagle M3, the Ultracam X was replaced in the following years. The Ultracam Eagle M3 belongs to the current state-of-the art cameras for photogrammetric measurements with 450 MP (Bühler et al. 2021). The improvements include a sensor pixel size of 4 µm x 4 µm, a focal length of 120.7 mm and a resolution of 26000 x 14000 pixels (Eberhard et al. 2021). Both Ultracam cameras acquire the four spectral bands red-green-blue (RGB) and NIR with a radiometric resolution of 14 bits. The camera positions are registered by differential global navigation satellite system (DGNSS) mounted at the camera with a nominal accuracy of 0.2 m. The orientation of the camera is recorded through an inertial measurement unit (IMU) with a nominal accuracy of 0.01° (omega, phi, kappa). This data simplifies the determination of interior orientation and the correct georeferencing and prevents tilts of the DSM.

The flights were conducted during the expected peak of winter (at approximately 2000 m) between March and April around midday to avoid large, shaded areas. The exact extent of each flight varied from year to year and is based on the flight route and weather conditions (Fig. 1). The captured region in 2017 covered 600 km² (Fig. 1, black polygon) and was considerably larger than in the following years. High costs and limited flight permissions resulted in the selection of a smaller main study area (250 km², red polygon) around Davos for the subsequent years.

Before the flights, reference points were marked with specially patterned tarps and measured by DGNSS with a vertical accuracy of 0.05 m. Because no reference points were acquired in 2017 and 2019, ten extra reference points on conspicuous road markings were measured in retrospect. Different characteristics of each flight are described in Table 1.

Table 1. Properties of the executed annual Ultracam flights during peak of winter.

Acquisition date	Sensor type	Reference points	Mean GSD [m]	Mean flight altitude [m above ground]	Notice
16 March 2017	Ultracam X	0	0.23	3430	Large, shaded areas, inaccuracies of NIR-band
11 April 2018	Ultracam Eagle M3	8	0.06	1780	Technical problems (airplane), heavily cloudy
16 March 2019	Ultracam Eagle M3	0	0.12	4040	Only RGB-bands, no NIR-band
6 April 2020	Ultracam Eagle M3	38	0.12	3970	Good conditions
16 April 2021	Ultracam Eagle M3	14	0.12	3910	few clouds in the east and west part, new snow

3.2 Reference dataset

3.2.1 Airborne laser scanner (ALS) from summer 2020

Calculating snow depths with photogrammetric methods requires an accurate snow-free reference dataset. For the study area, an ALS point cloud from summer 2020 was available (Federal Office of Topography swisstopo 2021a). The specified accuracies of at least 0.2 m in horizontal and 0.1 m in vertical direction comply with the requirements of accurate snow depth mapping. The point density of the ALS point cloud of at least 10 points m^{-2} and on average 20 points m^{-2} for all returns as well as 15 points m^{-2} for ground returns allows a rasterization of 0.5 m and the exact reconstruction of small-scale features as well as steep faces. The exact point classification enables the separation of vegetation, ground, buildings and water bodies. Correspondingly, a digital terrain model (DTM), a normalized ALS-DSM which only considered vegetation and a normalized-DSM which only took buildings into account were processed from the ALS point cloud. The ALS-DTM also served as a reference dataset to evaluate the accuracy of the snow depth maps through the comparison of snow-free areas.

3.2.2 Unpiloted aerial systems (UAS) photogrammetry 2018 and 2021

To analyse spatial snow depths of small catchments, UAS-derived DSMs are commonly used, given the flexible acquisition at a vertical accuracy better than 0.1 m (Bühler et al. 2016). In order to compare snow depths derived from airborne data to UAS derived ones, two UAS flights were carried out for a small subset (3.5 km²) in the Dischma Valley during the Ultracam flight campaigns in 2018 and 2021 (Fig. 1, green polygon). In 2018 there was a small-time lag (4 days) between UAS (eBee+ RTK) and airborne data acquisition. No significant snowfall, but slightly positive temperatures (0°C level at 2500 m) were registered in between. In 2021, the UAS acquisition was conducted simultaneously to the Ultracam flight by the WingtraOne drone with a 42 MP camera. The processing workflow of the UAS-derived DSMs was similar to the approach described in Eberhard et al. (2021) with the only difference that outliers of the point cloud (less than 3 depth maps) were excluded.

3.2.3 Manual reference points

The manually measured reference points during the Ultracam flights had the purpose of serving as GCPs or check points (CPs). Due to the time-consuming fieldwork as well as the avalanche danger, the number of reference points was limited, and they were often located close to roads in flat terrain. The ten points measured in retrospect at distinctive locations were valid as reference, although they have a lower reliability compared to directly measured reference points. In 2020, during low-level avalanche danger, 40 reference points could be placed well distributed at different elevations and aspects.

4 Methods

The creation of reliable and accurate snow depth maps consists of four steps (Fig. 2):

- Processing of airborne imagery and ALS point cloud
- Calculation of snow depths
- Creation and application of necessary masks
- Accuracy check of the finalized snow depth maps

The horizontal coordinate system CH1903+ LV95 and the height reference system LN02 were used for the processing of data. To ensure that the same coordinate system was used for all input data, conversions from other coordinate systems were carried out with the tool REFRAME (Federal Office of Topography swisstopo 2021b) and transformations available in ArcGIS Pro 2.7. The processing of airborne imagery was realized in Agisoft Metashape 1.6. It has proven its value in numerous snow-related studies (Avanzi et al. 2018; Bühler et al. 2016) and allows the processing of very large high spatial resolution airborne images (Eberhard et al. 2021; Meyer et al. 2022). The calculations and modifications of the snow depth values were realized in ArcGis Pro.

4.1 Processing workflow of airborne imagery

The processing of aerial images in Agisoft Metashape is based on the Structure from Motion algorithm (Koenderink und van Doorn 1991; Westoby et al. 2012). The general workflow is well-explained in various publications (Adams et al. 2018) and in the Agisoft manual (Agisoft LLC 2020). However, the existing framework conditions of this study, applying the new sensor Vexcel Ultracam in combination with such a large and heterogeneous study area are sparsely explored.

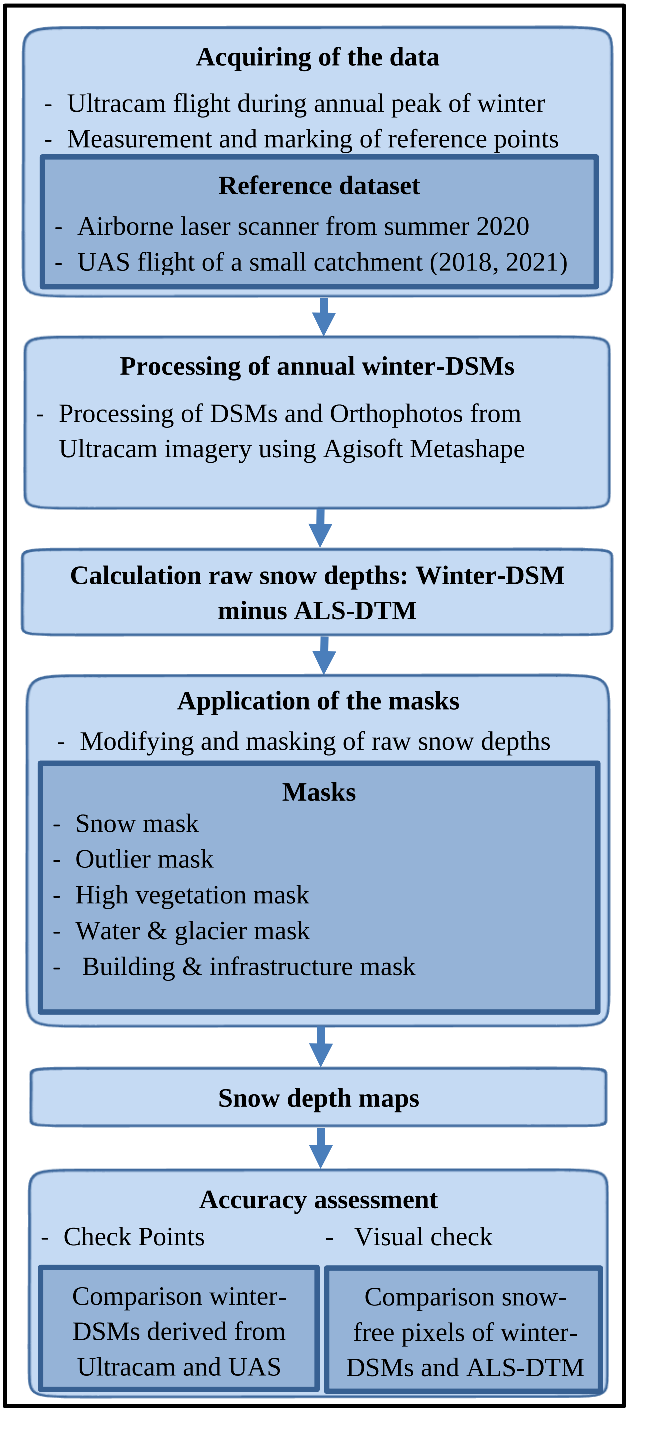

Figure 2. Flowchart illustrating all processing steps for the creation of snow depth maps.

Only Eberhard et al. (2021) successfully generated a winter-DSM derived from Ultracam imagery. Therefore, the workflow used in this study is based on Eberhard et al. (2021). However, the aim to use as few as possible GCPs to refine the orientation due to the limited availability of reference points required an adaption of this workflow.

The Vexcel Ultracam camera is calibrated, hence the interior orientation is known exactly. However, the application of the calibrated lens distortion parameters led to a large offset of the z-value in the resulting DSM of approximately 2 m. Therefore, the interior and exterior orientation were calculated in Agisoft Metashape during the bundle-adjustment process (Triggs et al. 2000). Subsequently, the parameters for the interior and exterior orientations (especially focal length) were improved by the application of two to five GCPs. The necessary number of GCPs and the influence of their distribution for an exact and reliable orientation was determined by a parameter study for the Ultracam flight in 2020, which was characterized by 40 well-distributed reference points (Table A1). The quality grade was ascertained by the calculated RMSE of the check points, which were not used for the orientation of the model (Agisoft LLC 2020). This approach has shown that only one GCP is sufficient for a correct orientation and determination of atmospheric distortions under favourable acquisition conditions. Using more and well distributed GCPs had no significant influence on the quality grade (Table 2). However, due to the high dependence on the precise measurement when using only one GCP, and the possibility of varying atmospheric distortions when using cloud-covered images, we recommend the use of two to five GCPs. Warps and tilts, which often occur using a low number of GCPs with a limited dispersion over the area, were avoided because of the availability of the exact coordinates of the shutter release points and the rotation angles of the camera.

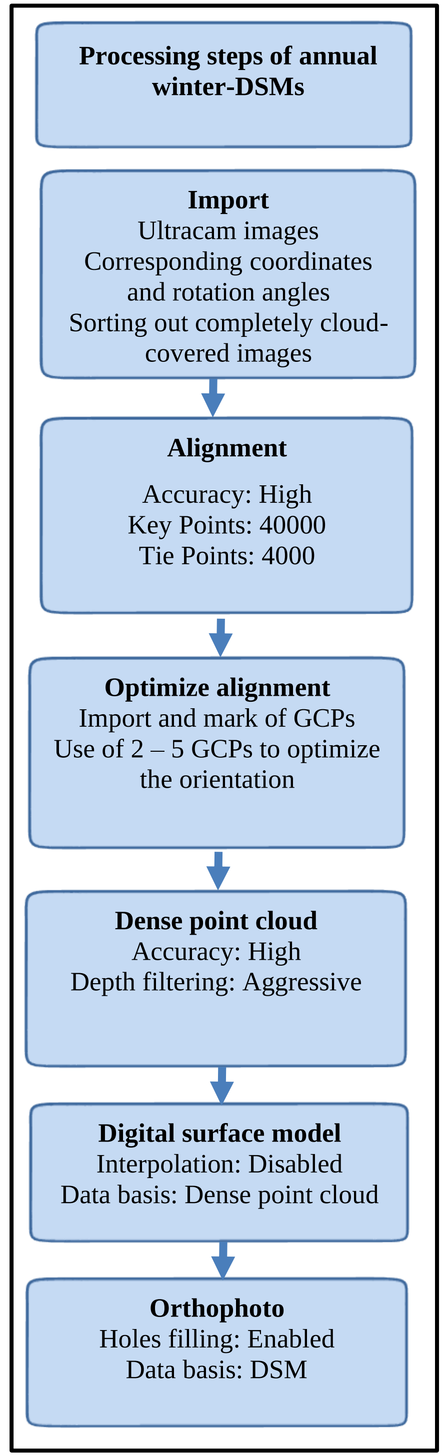

Figure 3. Flowchart illustrating the workflow generating the winter-DSMs on the basis of Ultracam images.

Table 2. Overview of the settings used and the corresponding accuracy (RMSE) for the parameter study for 2020.

Pre-calibration	Used dGNSS coordinates	Used rotation angles	Number and distribution GCPs	RMSE (Z; Total) [m]
✓	✓	✓	-	2.19; 2.20
✘	✓	✓	-	1.04; 1.08
✘	✓	✓	15	0.07; 0.15
✘	✓	✓	4 (Davos, Dischma, Sertig)	0.07; 0.155
✘	✓	✓	3 (Davos, Dischma, Frauenkirch)	0.08; 0.16
✘	✓	✓	1 (Davos)	0.08; 0.17

The final DSMs with a point density from 5 points m^{-2} (2017) over 20 points m^{-2} (2019 – 2021) up to 90 points m^{-2} (2018) and the corresponding orthophotos were exported with a spatial resolution ranging from 0.1 to 0.45 m depending on the average GSD. The workflow used is illustrated in Fig. 3 and further settings are described in Eberhard et al. (2021).

4.2 Creation of snow depth maps

The snow depths were calculated by subtracting the photogrammetric winter-DSM from the ALS-DTM resulting in snow depth maps with a spatial resolution of 0.5 m, using the resampled winter-DSMs. To avoid uncertainties based on misalignments between the winter-DSM and the ALS-DTM, we checked deviations of snow-free pixels in steep areas in each snow depth map. Since the deviations were small and the number of snow-free pixels in some years were limited, we did not perform a co-registration. The use of an ALS-DTM was preferred because a DSM would underestimate the snow depths in open areas with low vegetation (Eberhard et al. 2021; Feistl et al. 2014). In addition, photogrammetric methods often struggle in dense and steep forests as well as in settlements in our study area, where the ALS-DSM would have crucial advantages (Bühler et al. 2015).To get accurate and reliable snow depth maps, the application of various masks was required. Without the application of these masks, the average snow depth value of the study area would be overestimated by approximately 1 m, mainly caused by the forested areas.

The procedure for developing these masks is based on the approach of Bühler et al. (2015), improved by Bührle (2021) and contains a snow, an outlier, a high vegetation, a water and glacier mask as well as an infrastructure and building mask. However, the existing algorithm to calculate the masks was adapted due to the use of the better Ultracam sensor and the availability of an accurate and well-classified ALS point cloud. An important goal for the procedure is the consistent and reproducible creation of the masks (Fig. 4). Additionally, excluding regions with heavy cloud-cover and outlying areas led to more reliable snow depth values.

4.2.1 Snow Mask

The snow mask has the aim to modify calculated snow depths of snow-free areas to zero (Bühler et al. 2016). Therefore, each pixel of the corresponding orthophoto is classified as snow-covered or snow-free, using the Normalized Difference Snow Index (NDSI)(Dozier 1989; Hall et al. 1995) with a threshold around 0. This approach was applied for the years 2017, 2020 and 2021. A NDSI classification was not done in 2019 due to technical issues that prevented the recording of the NIR-band. In 2018, the NDSI method falsely classified pixels that exhibited snow mixed with soil as snow-free. Therefore, another classification method without the necessity of the NIR-band and a better operation in snow mixed with soil, was required. Since the blue band of snow exhibits higher reflectance than the red and green band (Eker et al. 2019) a threshold of the ratio between the blue and red band was used to determine the existence of snow. However, the values vary and depend on the strength of shadows, therefore the thresholds were manually determined by an expert. To ensure the reliability of this approach, 500 random points in open terrain in 2019 were selected and manually checked regarding their correct classification.

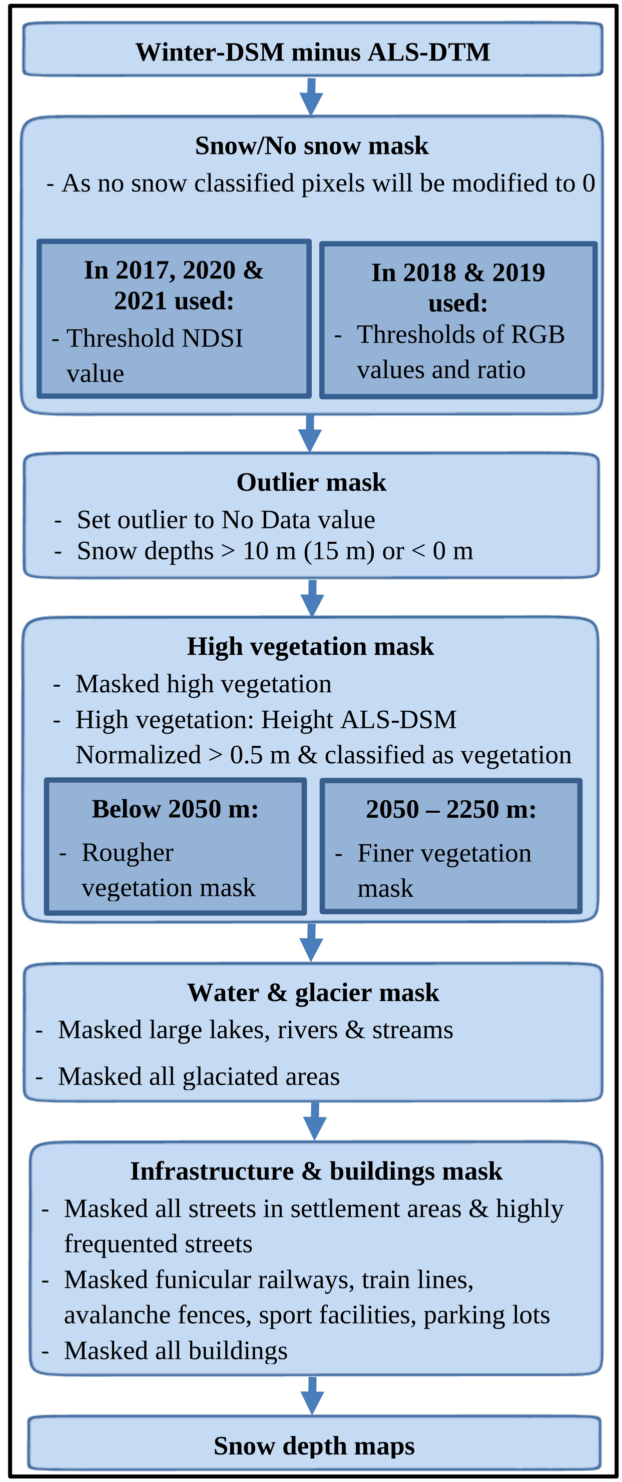

Figure 4. Flowchart illustrating the various masks used for the generation of reliable snow depth maps.

4.2.2 Outlier Mask

The outlier mask has the purpose to modify all unrealistic snow depth values, namely negative snow depths and extremely high snow depths above 10 m to No Data values. Only in the snow-rich year of 2019, the upper limit was adapted to 15 m.

4.2.3 High vegetation mask

Due to uncertainties in the actual snow depth and problems with photogrammetric methods, areas with high vegetation were masked out. High vegetation, defined as vegetation with a height above 0.5 m, were identified through the vegetation classification and the calculated object height using the ALS point cloud. Additionally, a generalisation of the high vegetation mask was required because wind, different sensor acquisition characteristics and the various capture times between ALS and Ultracam affected the extent of high vegetation. The algorithm used for the generalisation differed between a rougher mask below 2050 m, where dense forests are predominant, and a finer mask above 2050 m, where free-standing trees and bushes are prevalent.

4.2.4 Water and glacier mask

The water and glacier mask prevents unrealistic snow depth values on water and glaciated areas. Due to low water levels during peak of winter, the actual height of snow (HS) on frozen lakes is underestimated. Therefore, larger lakes, rivers and dominant streams were masked out. The data was obtained from the Swisstopo TLM3D geodata (Federal Office of Topography swisstopo 2021c). Another problem is the significant volume loss of glaciers (approximately 2 m per year) in recent years (GLAMOS - Glacier Monitoring Switzerland 2021). Accordingly, the calculated snow depths from 2017 to 2020 on glaciers are overestimated and therefore masked out (Linsbauer et al. 2021).

4.2.5 Infrastructure and building mask

The infrastructure and building mask prevents distorted snow depths caused by buildings and by temporary or moveable objects. Consequently, all buildings were completely masked out and infrastructure was partially masked. The buildings were derived from the classified point cloud of the ALS. The locations of technical constructions and infrastructure such as streets were obtained by the Swisstopo database. Railways, funicular railways, sport facilities, parking lots, all streets in settlement areas and main roads outside the settlements were masked out. Technical constructions like avalanche fences were also set to No Data. A very rough generalisation was used within dense settlements such as Davos, Arosa, and Klosters, whereas a finer generalisation was applied for areas beyond these settlements.

4.2.6 Masking Overview

Using all presented masks (Fig. 5) on the raw snow depth values resulted in the final snow depth maps. For the snow depth map 2020 around 67 % of all pixels remained in the snow depth maps. 28 % of the main study area was masked out as it belonged to high vegetation areas. Only less than 1 % of the pixels were masked out as outlier (Table 3; Table A2).

Table 3. Area [km^2] and percentage [%] of various masks, outliers and remaining snow depth values for the 2020 snow depth map.

	Water	**Glacier**	**Building & infrastructure**	**High vegetation**	**Outlier**	**Snow depth values**
Area [km^2]	1.1	2.7	6.6	60.6	1.7	161.3
Percentage [%]	0.5	1.2	2.7	25.9	0.7	69.0

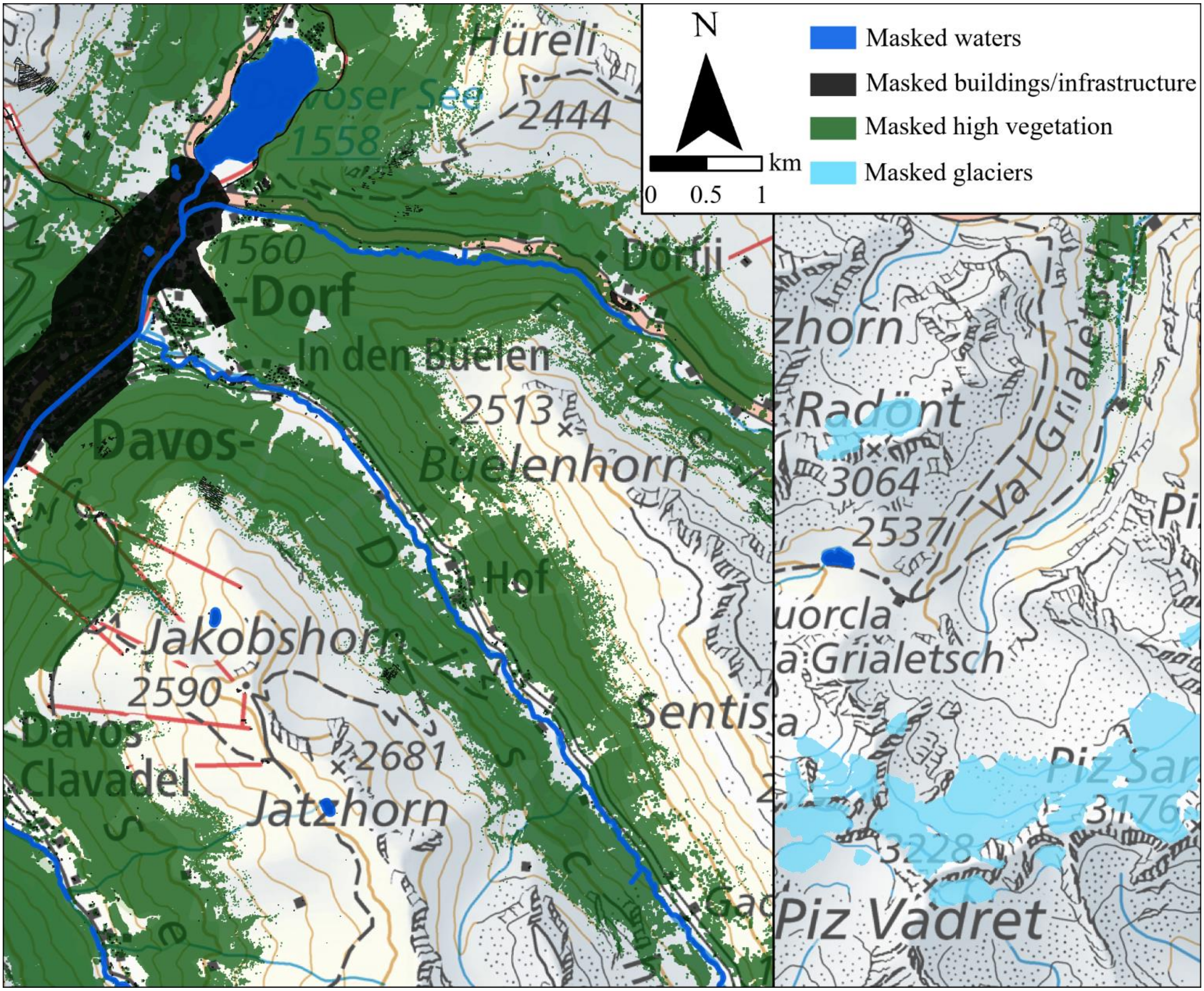

Figure 5. Spatial distribution of the masks used in selected extents of the main study area. Darkblue (water), light blue (glaciers), green (high vegetation) and black (buildings and infrastructure) polygons symbolize the different masks. Rivers are overrepresented for a better identification (map source: Federal Office of Topography).

4.3 Accuracy Assessment

An essential part of this study is an extensive accuracy assessment of the snow depth values. Due to the absence of spatially continuous ground truth datasets, we determined the accuracy compared to several available reference datasets. The accuracy assessment consists of five different methods which enabled a conclusive and spatially continuous evaluation of the annual winter-DSMs. The selected quality procedures differ between the years and depend on the availability of reliable reference data (Table 4).

- The first method uses independent **check points (M1)** as validation (Sanz-Ablanedo et al. 2018). Even though, the number of check points was limited, and they were predominantly not well-distributed over the entire study area, they are an important indicator for the correct orientation of the winter-DSMs.

- Due to their outstanding accuracy, **UAS-derived DSMs (M2)** serve as ground reference and enabled direct and spatial comparison with Ultracam data over a small area (Deschamps-Berger et al. 2020; Marti et al. 2016).
- **Visual checks (M3)** by an expert examined the plausibility of calculated snow depths and the correct application of the masks over the entire study area.
- Comparisons of snow-free areas on the winter-DSMs with the reference ALS exhibited further evaluations. **Method 4 (M4)** determined deviations on the **main roads** beyond settlements which were always snow-free (Fig. 6). Extreme outliers exceeding 3 m (approximately MBE ± 4 SD) were excluded, because bridges, tunnels and moveable objects led to higher deviations.

M4 was applied in most of the snow depth maps, except 2019. In 2019, the absence of the NIR-band in combination with puddles on the streets resulted in high deviations, which do not correspond to the actual accuracy. For a significant assessment, streets without puddles were manually digitalized and used as M4 in 2019.

- **Method 5 (M5)** considered deviations of **all other snow-free pixels (M5)** beyond settlements compared to the ALS-DTM. Pixels with vegetation heights exceeding 0.05 m were excluded. Moreover, occasional and temporal changes of objects and infrastructure occurred between the acquisitions of the winter DSMs and the ALS. Therefore, extreme outliers exceeding 3 m (approximately MBE ± 4 SD) were excluded. Limited snow-free areas beyond streets in the winters of 2018 and 2019 impeded a meaningful evaluation of snow-free pixels in these years.

Table 4. Overview of the accuracy assessment methods performed in the different years.

	2017	2018	2019	2020	2021
M1: Check Points	×	✓	(✓)	✓	✓
M2: UAS	×	✓	×	×	✓
M3: Visual check	✓	✓	✓	✓	✓
M4: Comparison ALS on streets	✓	✓	(✓)	✓	✓
M5: Comparison ALS beyond streets	✓	×	×	✓	✓

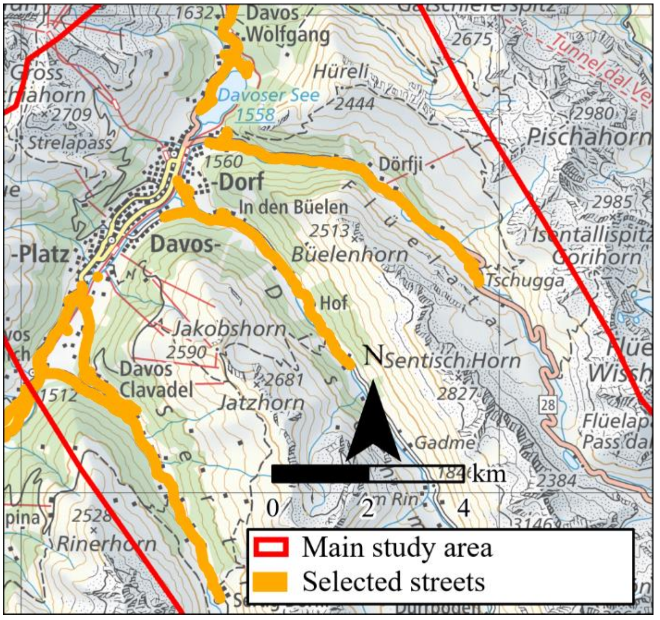

Figure 6. Overview roads used (orange lines) for the accuracy assessment method 4, lines are overrepresented for better identification (map source: Federal Office of Topography).

The quantitative procedures were evaluated by various commonly-used statistical quality grades such as mean bias error (MBE), standard deviation (SD), RMSE, median (MdBe) and normalized median absolute deviation (NMAD) (details in

Eberhard et al. 2021 and in Höhle und Höhle 2009). The significant impact of a few pixels with high deviations caused by the distortions described above led to the calculation of quality grades, excluding deviations beyond the confidence interval (MBE +- 2 SD).

Finally, since the accuracy of the snow depth values also dependents on the **reference ALS-DTM**, we have examined the specified accuracy (Z = 0.1 m) comparing 24 reference points (see section 3.2.3) on snow-free areas with the ALS-DTM.

5 Results and validation

5.1 Accuracy Assessment

The quantitative part (M1, M2, M4, M5) of the accuracy assessment compares the deviations of the winter-DSM to a selected reference dataset. Due to the horizontal accuracy of the check points (M1) of the winter-DSMs was approximately 0.1 m in each year, which is also influenced by inaccuracies of the GNSS, we especially focused on the vertical accuracy. The RMSE value comparing the ALS-DTM to 24 reference points of 0.03 m demonstrates the high reliability of the reference ALS. The achieved accuracy of the reference-DSMs derived from UAS was identified by using check points with a RMSE of 0.06 m (2021) and 0.1 m (2018).

5.1.1 2017

The accuracy assessment of the winter-DSM 2017 calculates RMSE values of 0.26 m on open streets and 0.3 m on snow-free pixels after outlier removal (MBE ± 2SD) (Table 5). Resulting dispersions of method 4 (SD = 0.33 m, NMAD =0.28) and method 5 (SD = 0.42 m, NMAD =0.32) have considerably higher values compared to the other years (see section 3.1; Table 1). The same result can be clearly seen at the significantly larger interquartile range of the winter-DSM in 2017 in Fig. 10. Additionally, Fig. 7 shows the difference of the accuracy and the corresponding dispersion between Ultracam X and the successor Ultracam Eagle M3. The impact of the higher deviations is evident regarding the high number of outliers (3%; negative snow depths) in steep and heterogenous terrain. Furthermore, inaccuracies of the NIR-band led to insufficient classification of the snow masks. Accordingly, numerous pixels on streets, in transition zones of snow-free to snow-covered and in shaded areas are falsely classified as no snow.

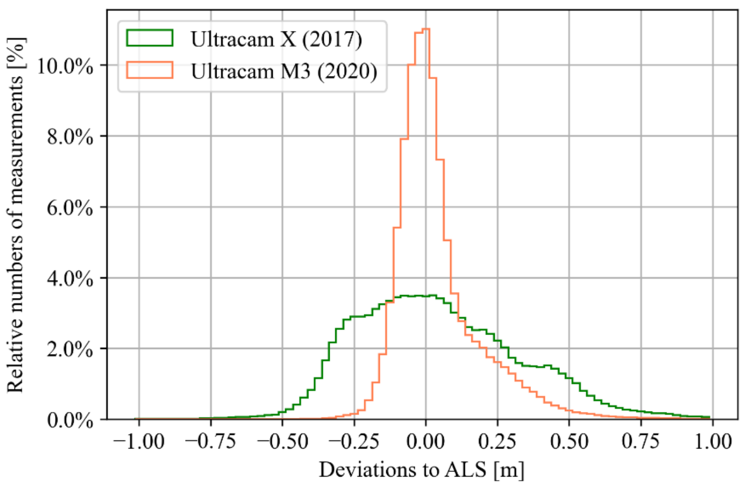

Figure 7. Comparison of the dispersion of deviations on streets to ALS between Ultracam X (green, 2017) and Ultracam Eagle M3 (light red, 2020).

5.1.2 2018

In 2018, large cloud-covered areas were excluded from the processing. Therefore, missing images and partly cloud-covered images caused less overlap in these regions. Nevertheless, the deviations of the ten check points (RMSE 0.13 m) and the comparison with the UAS-derived DSM (RAW = 0.12, Filtered = 0.09 m) demonstrate a very high accuracy of the winter-DSM (Table 5). The low aspect-dependency of the deviations between UAS and Ultracam (Fig. 8) can be explained by the delay in capture time and therefore compression of the snowpack on southern slopes due to mild temperatures and strong solar radiation. The median of method 4 (RAW = 0.08, Filtered = 0.09) shows a slight overestimation of the snow depths, which especially occurred south of Davos, close to cloud-covered areas. Despite these overestimations, the RMSE (RAW = 0.18, Filtered = 0.16) of the deviations on roads also proves the spatially very high reliability of the winter-DSM. The classification of snow-covered pixels worked reliable, only isolated pixels in wet snow avalanches, exhibiting a snow-soil mixture, were falsely classified.

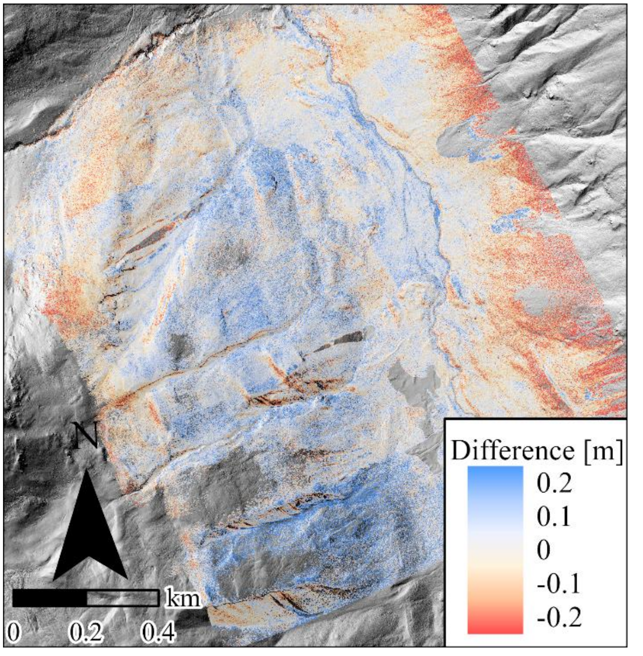

Figure 8. Difference calculation of the DSMs around the Schürliaalp derived from Ultracam data and UAS in 2018.

5.1.3 2019

The occurrence of technical errors on the airplane prevented the capture of the NIR-band, which can decrease the successful reconstruction of low-contrast snow surfaces and accordingly the accuracy of the DSM. However, no significant influence on the reconstruction or accuracy of the DSM was determined. This high accuracy is confirmed by evaluations of the RMSE of the check points (0.07 m) and especially the RMSE of the manually digitalized snow-free areas (Filtered = 0.11 m) (Table 5; Fig. 10). Using the snow–mask also led to a high-quality grade of more than 99 % correctly classified pixels (method described in section 4.2.1).

5.1.4 2020

The capture of the aerial images in 2020 was characterised by perfect acquisition conditions. Consequently, the winter-DSM in 2020 evince a very high accuracy of around 0.1 to 0.15 m, determined by the use of 36 well-distributed check points, which show a RMSE of 0.07 m (Table 5). The RMSE values of method 4 also indicate a high accuracy (RAW = 0.19, Filtered = 0.13). Furthermore, the large snow-free areas in 2020 enable a representative accuracy assessment of method 5 which considers deviations in different elevations and slopes. The RMSE of filtered deviations (0.18 m) in combination with the NMAD (0.16 m) of method 5 shows the high reliability of the winter-DSM in the entire study area and in steep terrain. The deviations of M5 in extremely steep areas exceeding 40° (Filtered RMSE = 0.3 m) confirmed, that the quality of the winter-DSM decreases with increasing steepness, but is still high (Bühler et al. 2015; Meyer et al. 2022).

5.1.5 2021

In 2021, the surface above 1800 m a.s.l. was covered by a new snow layer, which caused less contrast during the Ultracam recording. Despite these difficult conditions, the check points indicate a similar high accuracy as in 2020 (RMSE = 0.12 m). The RMSE (RAW = 0.14, Filtered = 0.12) values of the comparison between the DSMs derived from Ultracam and UAS also show very good results, with a slight tendency to underestimate the winter-DSM (Fig. 9). The underestimation is characterised by a negative median (Filtered = -0.09). The median values of method 4 (RAW and Filtered =0) and method 5 (RAW and Filtered = 0) show however, that this underestimation is a local problem and not valid for the entire study area. The RMSE value calculated with method 4 (Filtered = 0.11 m) and 5 (Filtered = 0.16 m) demonstrates the very high accuracy of the snow depths (Table 5). Additionally, partly cloud-covered areas led to no significant increase of the dispersion, which is shown in the low NMAD values of method 4 (RAW = 0.09) and method 5 (RAW = 0.15).

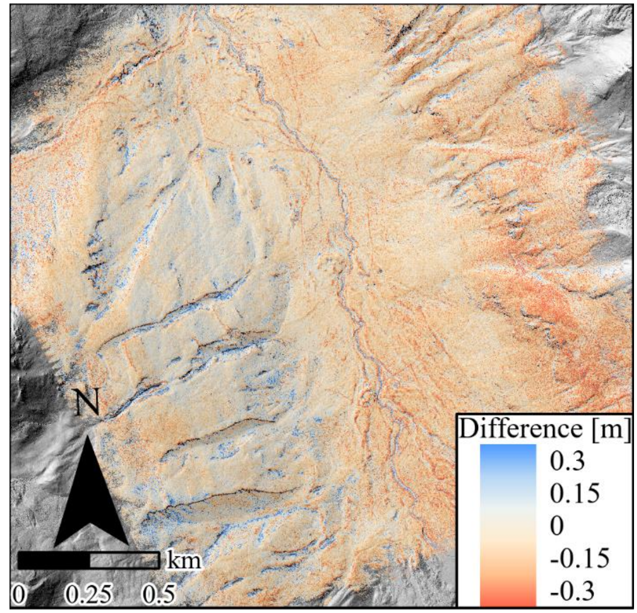

Figure 9. Difference calculation of the DSMs around the Schürliaalp derived from Ultracam data and UAS in 2021.

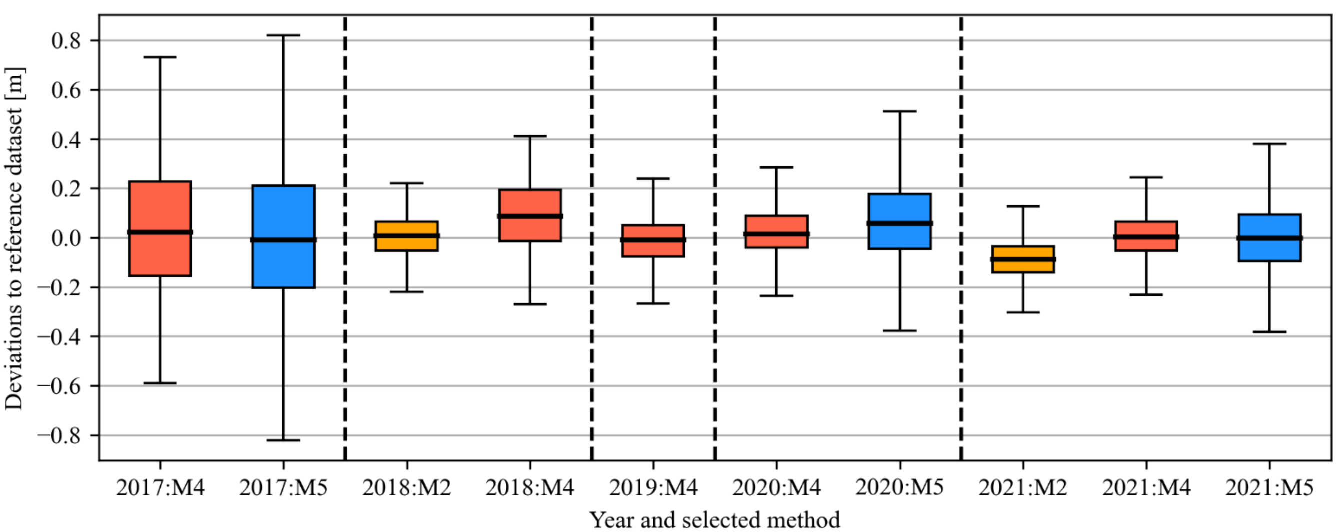

Figure 10. Box plots of the filtered deviations (MBE ± 2SD). Used Methods: M2 (orange), M4 (red) and M5 (blue) for each year.

Table 5. Overview and comparisons of the quality grades of the winter-DSMs; Column “Filtered” excluded outliers (MBE ± 2 SD).

		M1: Check Points	**M2: UAS**		**M4: Comparison ALS (streets)**		**M5: Comparison ALS (snow-free pixels)**	
		RAW	**RAW**	**Filtered**	**RAW**	**Filtered**	**RAW**	**Filtered**
2017	MBE[m]	×	×	×	0.07	0.045	-0.02	0
	SD[m]	×	×	×	0.33	0.26	0.42	0.3
	RMSE[m]	×	×	×	**0.33**	**0.26**	**0.42**	**0.3**
	MdBE [m]	×	×	×	0.03	0.02	-0.02	0
	NMAD [m]	×	×	×	0.28	0.28	0.32	0.3
	Number measurements	×	×	×	347’068	336’135	15’003’508	14’355’536
2018	MBE[m]	×	0	0	0.07	0.08	×	×
	SD[m]	×	0.12	0.09	0.16	0.14	×	×
	RMSE[m]	**0.13**	**0.12**	**0.09**	**0.18**	**0.16**	×	×
	MdBE [m]	×	0	0	0.08	0.09	×	×
	NMAD [m]	×	0.09	0.09	0.16	0.15	×	×
	Number measurements	10	7’471’650	6’949’690	132’558	127’191	×	×
2019	MBE[m]	×	×	×	×	0	×	×
	SD[m]	×	×	×	×	0.11	×	×
	RMSE[m]	**0.07**	×	×	×	**0.11**	×	×
	MdBE [m]	×	×	×	×	0	×	×
	NMAD [m]	×	×	×	×	0.09	×	×
	Number measurements	6	×	×	×	25’944	×	×
2020	MBE[m]	×	×	×	0.06	0.04	0.09	0.07
	SD[m]	×	×	×	0.18	0.12	0.27	0.17
	RMSE[m]	**0.07**	×	×	**0.19**	**0.13**	**0.28**	**0.18**
	MdBE [m]	×	×	×	0.02	0.02	0.07	0.06
	NMAD [m]	×	×	×	0.10	0.09	0.17	0.16
	Number measurements	40	×	×	221’087	214’114	30’933’482	29’522’927
2021	MBE[m]	×	-0.08	-0.08	0.03	0.01	0.02	0
	SD[m]	×	0.12	0.08	0.18	0.11	0.27	0.16
	RMSE[m]	**0.12**	**0.14**	**0.12**	**0.19**	**0.11**	**0.26**	**0.16**
	MdBE [m]	×	-0.09	-0.09	0	0	0	0
	NMAD [m]	×	0.08	0.08	0.09	0.09	0.15	0.14
	Number measurements	19	16’386’474	15’987’661	227’907	217’453	6’342’785	6’141’131

5.2 Snow depth maps

Despite varying and partly difficult acquisition conditions (section 3.1) as well as some extremely steep and complex areas, on average, more than 99 % of the snow depth values in not-masked areas were reconstructed. Only in the winter-DSM from 2017, the image matching failed in few overexposed or shaded regions. The high rate of success enabled the spatially continuous snow depth mapping of open areas around Davos. The spatial resolution of the maps (0.5 m) and the orthophotos (0.25 m) provide an excellent overview of the snow depth distribution within the study area. The existing level of detail shows numerous small-scale features over a large area and demonstrates the high variability of snow depths even within small distances. Special characteristics of the study area are the strongly varying average snow depths and snow cover. The average snow depth values of the selected years ranged from 1.29 m in 2017 to 2.36 m in 2019 (Table 6). Comparing the 2019 and 2020 snow depth maps, significant differences in snow depth distribution and related features can be seen (Fig. 11). In 2019, the study area was almost completely snow-covered, exhibited numerous regions with high snow depths exceeding 3 m and was characterised by the occurrence of many slab avalanches. In contrast, the average snow depth in 2020 was considerably lower (1.42 m). The area was often characterised by snow-free slopes below 2400 m a.s.l. in southern aspects as well as numerous glide-snow and wet-snow avalanches. Furthermore, the aspect-dependence of the snow depths was more decisive in 2020 than in 2019.

Table 6. Overview average snow depths [m] and standard deviation [m] of each annual snow depth map.

Year	2017	2018	2019	2020	2021	Mean
Average	1.29	1.50	2.36	1.42	1.71	1.66
SD	0.87	0.83	1.33	1.01	1.11	1.03

Despite the high difference of the average snow depth values between these two years, similar patterns in the relative snow depth distribution and occurrence of special features are identifiable. In general, the snow depths in both years increases with rising elevation until a certain level close to ridges or peaks. Higher snow depths are more frequently found on northern aspects compared to south-facing slopes which shows the aspect-dependence of snow depths. Furthermore, higher and lower relative snow depths of both snow depth maps occurred at similar locations (Fig. 11).

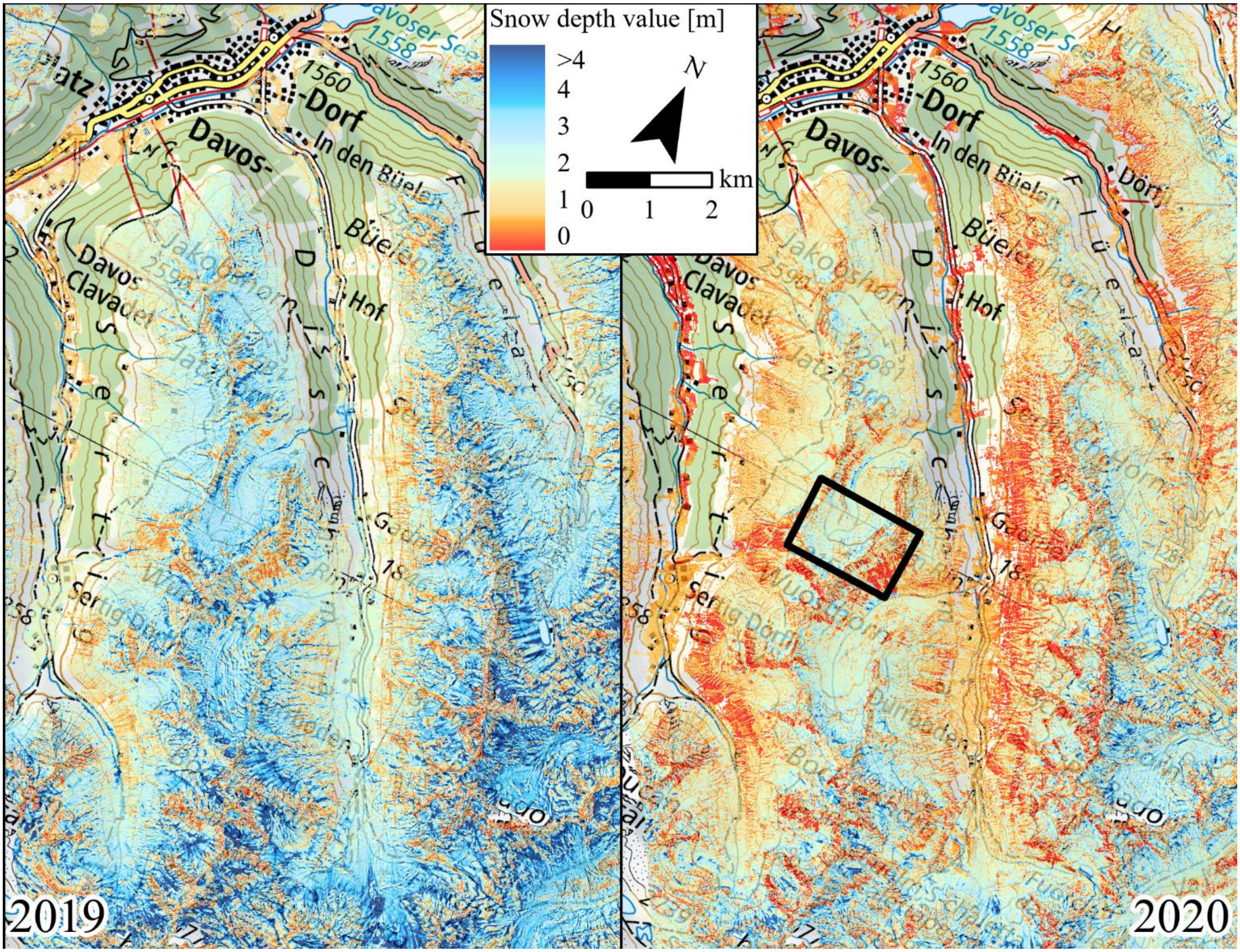

Figure 11. Comparison of an extent of snow depth maps from 2019 and 2020 during corresponding peak of winter. The black polygon shows the location of the selected small catchment for a more detailed comparison between the available snow depth maps (Fig. 12) (map source: Federal Office of Topography).

We further investigated the snow distribution patterns by comparing the relative snow depth distribution between the years. The normalized snow depth values of each year were calculated by the relation of the HS in contrast to the average snow depth of the selected area in the corresponding year. The normalized snow depth maps have the advantage of being independent from differences in the absolute snow depth between the years, which enables a better overview of the actual snow depth distribution. As depicted exemplarily in Fig. 12, we observed similar distribution patterns between all years. Generally, higher relative snow depths often occurred at deposition zones of avalanches, along terrain edges in wind-protected zones and within sinks. Lower snow depths were frequently observed on slopes exceeding 35°, in wind-exposed areas and in the release zones of avalanches (see also 6.2.3). However, a few features such as avalanches in certain tracks only occurred in some years.

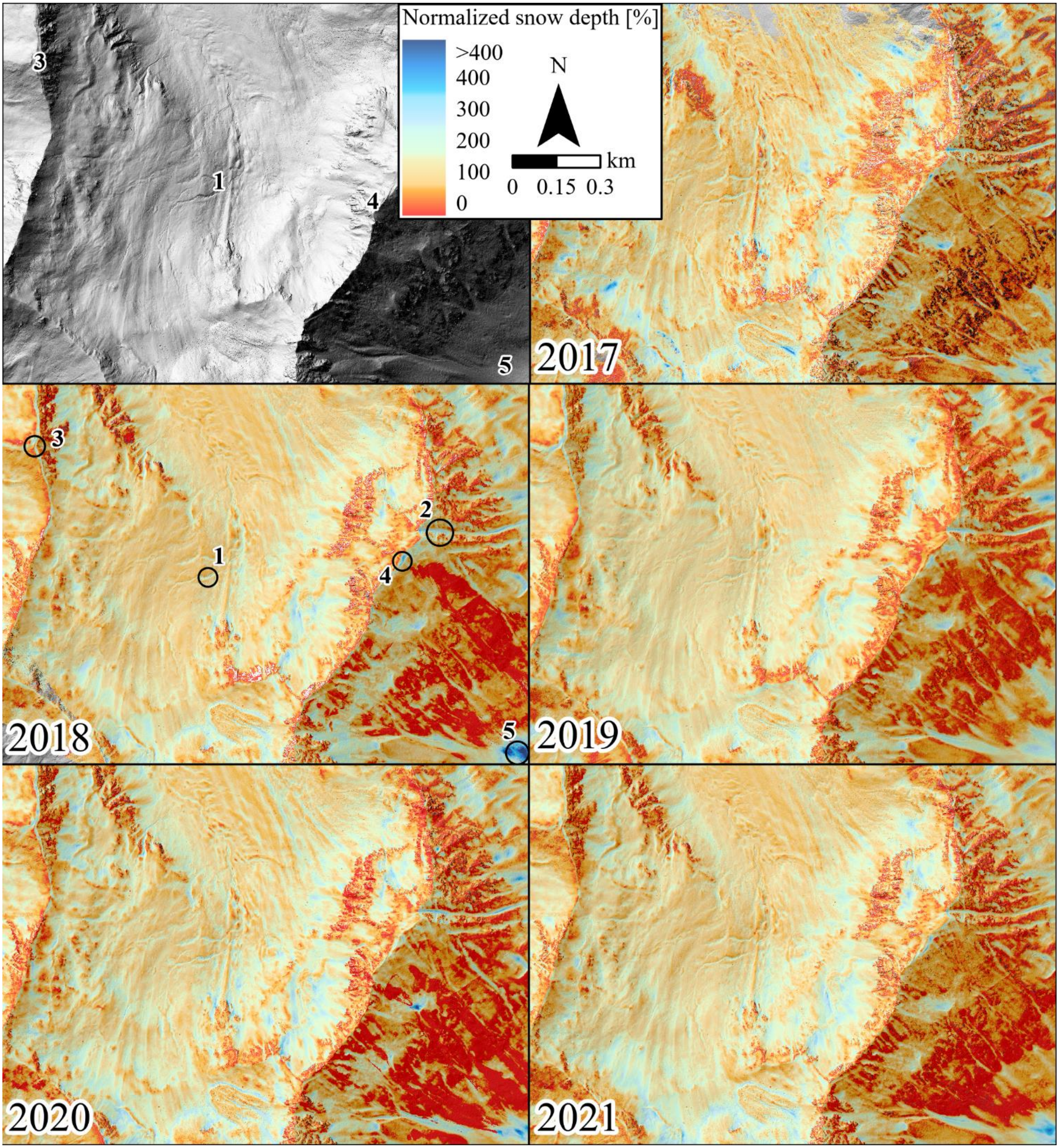

Figure 12. Comparison of the normalized snow depth maps of the 5-year period (2017 – 2021) during peak of winter in a small catchment (3 km²) close to Börterhorn. Numbers in the hillshade locate different special features, which demonstrate the existing grade of detail: 1. Filled small creeks; 2. Filled drainages in an extremely steep area close to Börterhorn; 3. remarkable cornice between Tällifurgga and Witihüreli; 4. Cornice between Wuosthorn and the Börterhorn; 5. Deposition zone of avalanches.

The detailed detection of numerous avalanches by means of the snow depth maps and corresponding orthophotos is a salient characteristic of the data. In particular, glide-snow avalanches, striking slab-avalanches and deposition zones of wet-snow avalanches can be identified. The investigation of the snow depth distribution around the fracture line enables the calculation of the release height. Exemplary shown in Figure 13, the release height of this slab avalanche was approximately 0.95 m.

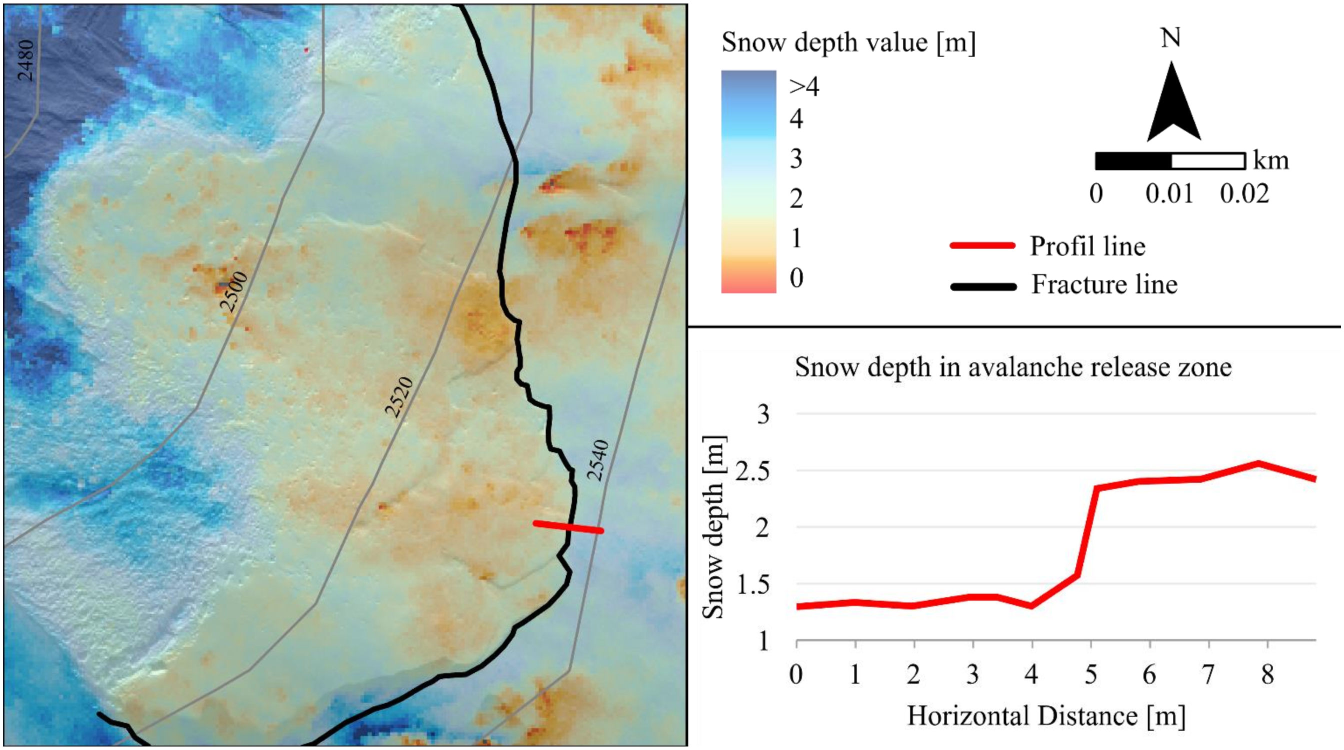

Figure 13. Overview of the snow depth distribution of the release zone of a slab-avalanche close to the Börterhorn (Dischma Valley) captured by the Ultracam in 2019; red line symbolises a height profile showing the course of snow depth values vertical to the fracture line; the prominent difference in snow depths indicates the release height of around 0.95 m.

To present additional applications of our snow depth maps, we exemplarily assessed snow depth distribution around different avalanche protection structures. Therefore, the workflow was slightly adapted by unmasking the avalanche fences. In 2019, the Ultracam recording was shortly after a large snowfall (1.3 m new snow at Weissfluhjoch within 7 days) during a snow-rich winter. The orthophoto and corresponding snow depth map shows that large parts of the release-zone avalanche fences, south of the wind-drift snow fences (1), were completely buried as snow accumulated up to 6 m (Fig. 14). The avalanche fences close to the ridge (2) were also covered by a prominent cornice with a snow height of 5.5 m.

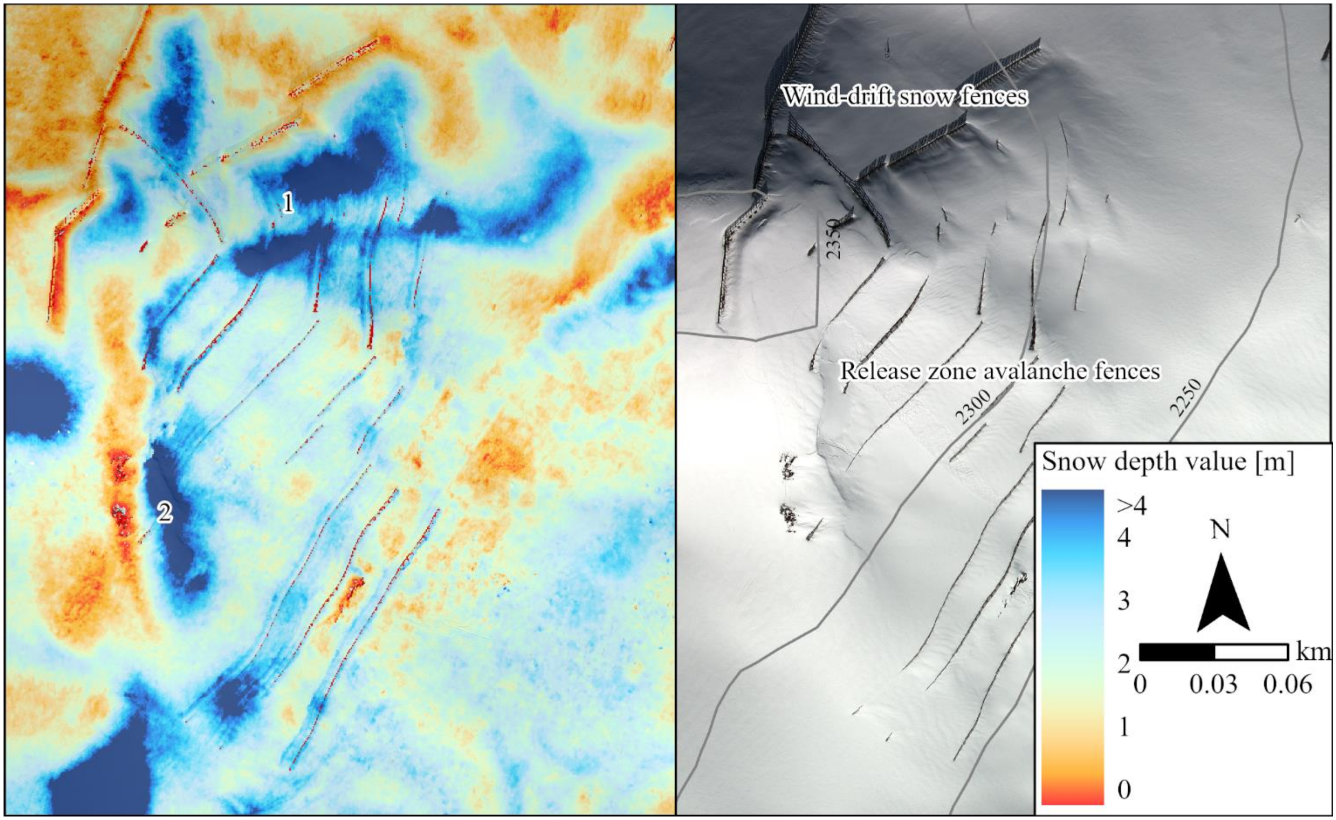

Figure 14. Snow depth distribution and corresponding orthophoto around different avalanches fences at the Grüeniberg captured by the Ultracam flight on the 16th of March 2019. The numbers 1 and 2 symbolize buried avalanche fences with high snow depths exceeding 5 m.

We also compared the average snow depth value of the different snow depth maps (core area) with the punctual snow depth measurements from the eight AWS around Davos, which are well distributed at different elevations and aspects in our study area (Fig. 1). Despite the large differences in snow heights between the years, the average value of all AWS was similar to the average value (+/- 0.07 m on average) derived from our snow depth maps (Fig. 15). Only in 2018, when the main part of the higher mountains was cloud-covered, our value was considerably lower (- 0.22 m) compared to the mean of the snow depth measurements from AWS.

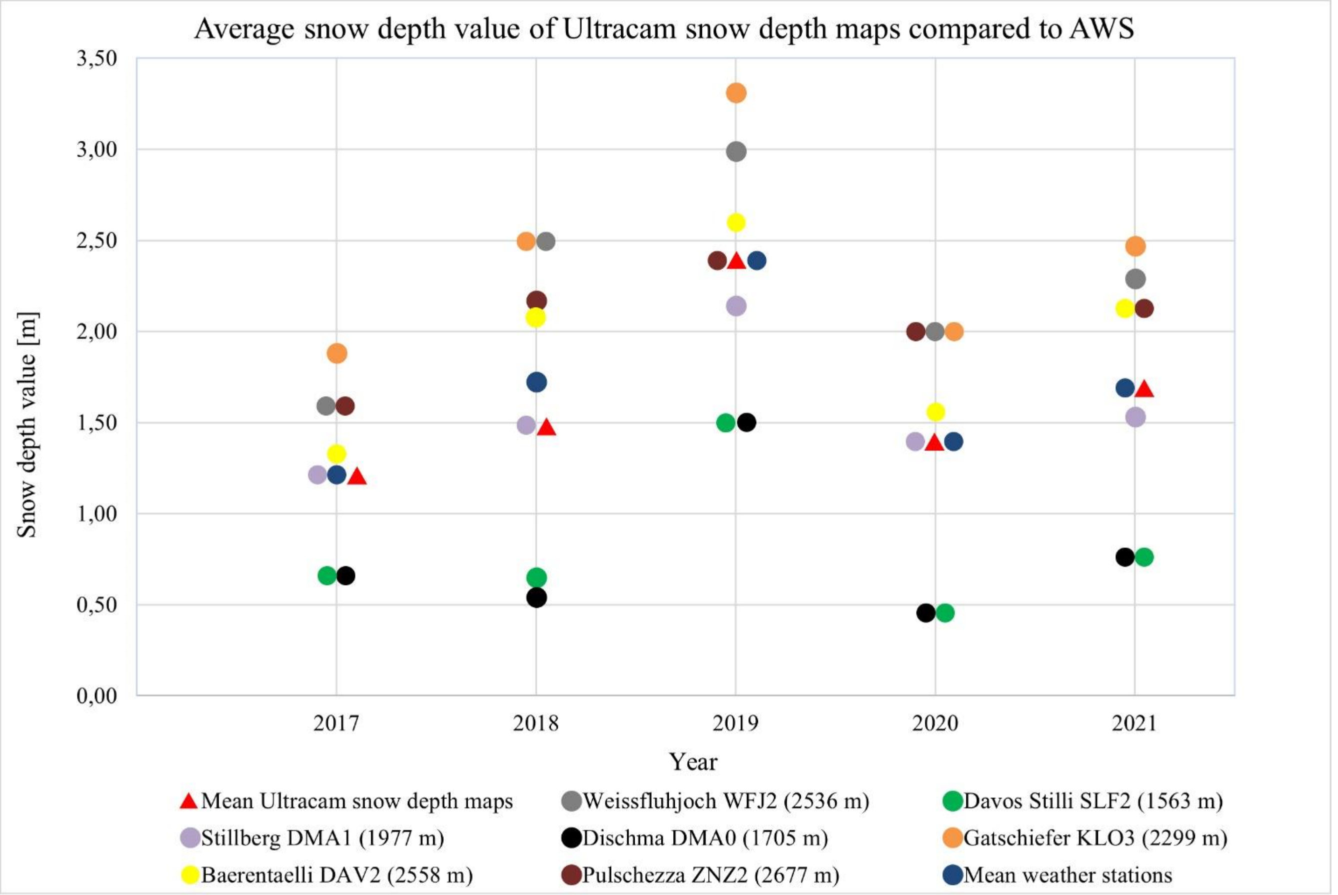

Figure 15. Average snow depth value from the Ultracam snow depth maps (red triangle, core area) compared to snow depth measurements from automatic weather stations (circles) during the Ultracam flights. Locations of the AWS are shown in Fig. 1. Blue circle symbolises the mean of all AWS snow depth measurements.

AWS snow depth measurements are supposed to yield typical snow height. Hence, finding a suitable location for a new AWS is a matter of finding an ideal location with representative snow height in the area of interest. To facilitate this decision-making process, SLF developed a model, taking into account snow depth, to assess the suitability for a new station in the Dischma Valley. Regarding the snow depth distribution, the model assesses the representativity of the measured snow depth for the area (Fig. 16). In addition, the model also considers different topography parameters such as roughness, avalanche danger (Bühler et al. 2022) and slope gradient.

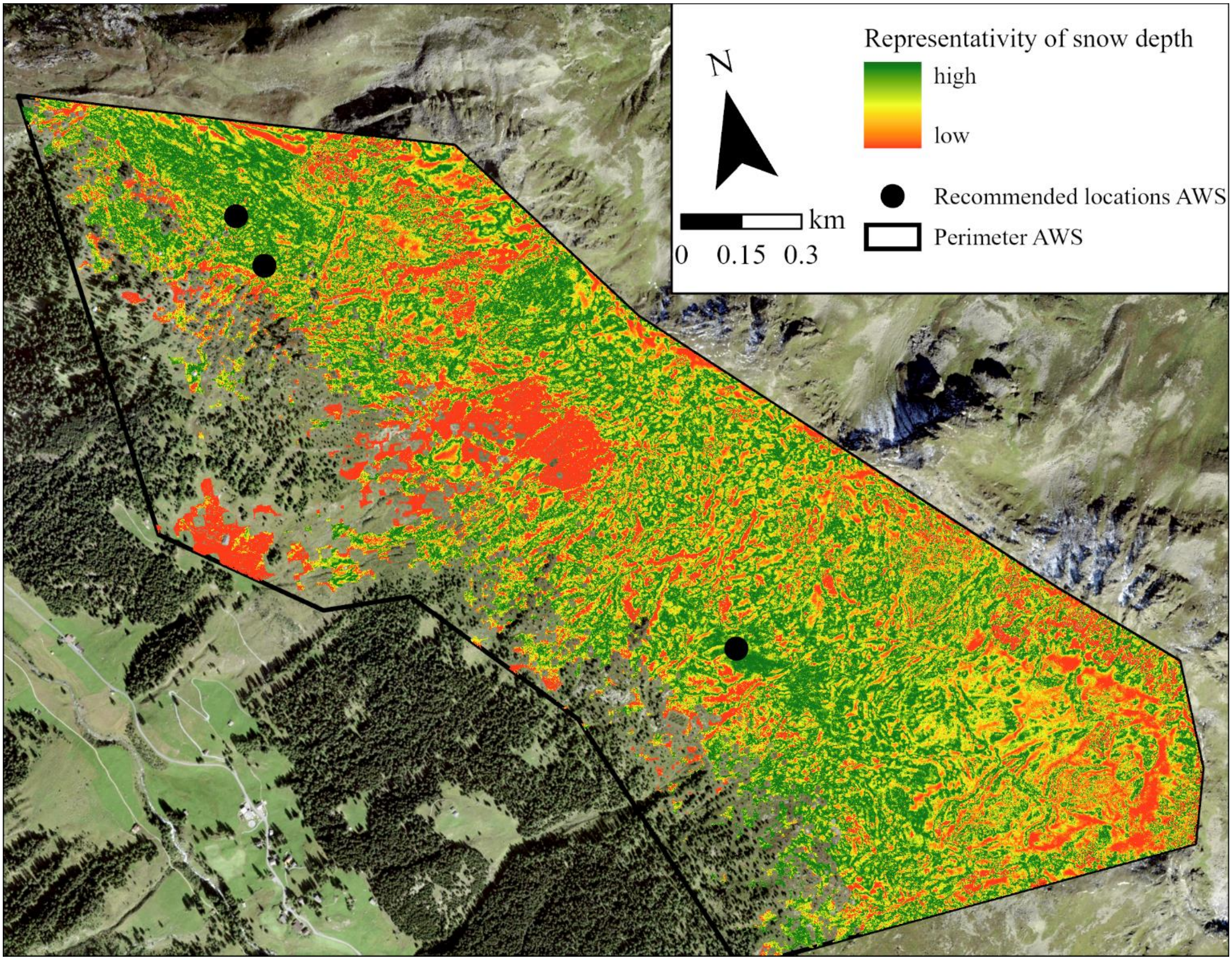

Figure 16. Representativity of punctual snow depth measurements (possible locations for AWS) for the entire perimeter (black polygon) derived from airplane snow depth maps. Black circles symbolise predefined locations for the AWS. The south location was finally selected due to its high representativity (dark green), low avalanche danger and flat terrain for the new AWS Lukschalp (map source: Federal Office of Topography).

6 Discussion

In this study we processed the data from the annual Ultracam flights (2017 to 2021) to snow depth maps. We investigated the necessary processing steps to derive accurate winter-DSMs, to apply required masks and to assess the characteristics of the resulting snow depth maps. We analysed the accuracy and validity of the resulting winter-DSMs and used the snow depth maps for different applications. In this section, we discuss the obtained results.

6.1 Processing of snow depth maps

This study focussed on the accurate and consistent processing of large-scale snow depth maps under different acquisition conditions with the new Vexcel Ultracam sensors over a period of five years. We have observed a significant quality increase from the Vexcel Ultracam X to the successor Eagle M3 due to its higher GSD and better radiometric characteristics. Data from the Ultracam X in 2017 exhibited errors in the NIR-band, which complicated the classification of snow-free pixels. The RGB-sensor of the Ultracam X was partly overexposed, hence Agisoft Metashape had problems to find matching points in few sunlit snow areas. The accuracy assessment in 2017 shows that the RMSE (~ 0.25 m) of the winter-DSM is significantly poorer than in the following years (Table 5; Fig. 10), which is no noticeable advance compared to other studies (Bühler et al. 2015; Nolan et al. 2015).

With the new Vexcel Ultracam Eagle M3 sensor, Agisoft Metashape was able to reconstruct almost the complete surface, even in heavily shaded areas, on surfaces covered by fresh snow as well as in partly cloud-covered regions. A similar successful processing of small catchments was achieved by Meyer und Skiles (2019). However, our approach still reveals a significant progress in photogrammetric snow depth mapping compared to other large-scale snow depth maps from previous studies (Bühler et al. 2015; Nolan et al. 2015). Using the Ultracam Eagle M3 also resulted in a considerable better GSD under similar flight altitudes compared to recent studies (Meyer et al. 2022). The better GSD enables the exact processing of snow depth maps with a spatial resolution of 0.5 m, which is better than previous large-scale snow depth maps and required to capture small scale distribution pattern accurately (Miller et al. 2022). The performance of extensive and significant accuracy assessments has shown a high reliability of the processed winter-DSM based on the Vexcel Ultracam Eagle M3 sensor with an accuracy of approximately 0. 15 m (Fig. 10). The accuracy assessment of the reference ALS-DTM compared to reference points (RMSE 0.03 m) has also demonstrated its high reliability. Therefore, the accuracy achieved in the winter-DSMs corresponds approximately to the actual accuracy of the calculated snow depth values. These accuracies of the snow depths match with the best results in Eberhard et al. (2021) and Meyer et al. (2022).

The strength of the presented workflow is the robustness which is demonstrated through the quality grades of the snow depth maps despite difficult and complex acquisition conditions in high-mountain regions. In addition, excellent acquisition conditions such as in the year 2020 resulted in no significant improvements of the quality metrics.

A crucial disadvantage of our workflow compared to the one of Meyer et al. (2022) is the necessity of 2 to 5 GCPs. Little effort was needed to measure the GCPs in the present study area due to the vicinity to the settlement, but this might be a limitation elsewhere. This could be solved by using a global coordinate system, but first experiences have shown that the accuracy is lower and less reliable compared to our workflow. Under consideration of this limitation, the procedure is applicable on different study areas.

Compared to the more expensive ALS-derived snow depth maps (Bühler et al. 2015; Deems et al. 2013; Painter et al. 2016) our computed metrics demonstrate an equal accuracy. However, in areas with high vegetation or dense forests it is currently not possible to derive snow depths through photogrammetry. Different approaches have been proposed to obtain snow depth with photogrammetric methods within forested areas (i.e. Broxton und van Leeuwen 2020; Harder et al. 2020), yet the steep slopes in combination with dense forests around Davos impeded the processing.

To counteract wrong values in those problematic areas, a similar masking approach to ours was previously applied in Bühler et al. (2015), but the algorithm we used has been considerably improved and is more reliable. The masks that we processed consistently and reproducible, are characterised by a high accuracy, but also exhibit little errors and limitations. In total, the percentage of incorrectly masked areas amounts to less than 1 %, which is considered satisfactory. The errors include for example snow-covered pixels in heavily shaded areas and snow mixed with soil falsely classified as no snow. Additional errors encompass new buildings, ignored single trees or environmental changes caused by mass movements. As those changes are inevitable in our study and the values only account for a small proportion of our masks, we assess their effects as negligible. The transferability of the masks to other study areas depends on the data availability of existing forests and settlements.

6.2 Applications

The remarkable characteristics of the snow depth maps and the corresponding orthophotos enable new possibilities for various applications in science and practice: The assessment and prevention of natural hazards, research on snow depth distribution processes and snow-hydrological models as well as other measurement methods. In the following sections we would like to discuss the relevance and potential impact of our work on selected applications.

6.2.1 Natural hazards

The investigation of natural hazards such as snow avalanches or snow loadings on buildings can benefit from the presented snow depth maps and the approach applied. Studies of Bühler et al. (2019), Hafner et al. (2021), Eckerstorfer et al. (2019) and Leinss et al. (2020) have already demonstrated the importance and limitations of manual as well as automatic large-scale avalanche mapping with satellite data. On a smaller scale Korzeniowska et al. (2017) proved the automatic detection of avalanches on the basis of orthophotos derived from airborne photogrammetry (sensor ADS80). Due to better radiometric characterisations and better spatial resolution of our orthophotos, even more details could be obtained than in previous studies. Furthermore, different studies (i.e. Peitzsch et al. 2015) have already suggested that the locations of glide-snow avalanches are often similar between winters. Our data series confirms this finding.

As exemplary shown in Fig. 13, the high-resolution orthophoto allows for the exact identification of snow avalanches and associated release and deposition zones over larger regions. In numerous cases, the detection of the fracture line of an avalanche is possible as well. Consequently, the snow depth distribution around the avalanche fracture line can provide meaningful information about the release height and volume. However, release zones covered by new or wind-drifted snow, or avalanches released in extremely steep and complex terrain can be difficult to identify. Nevertheless, these snow depth maps are the first study to enable the determination of release heights of distinctive avalanches within larger regions. Since so far only individual studies with UAS were able to accurately identify the release height (Souckova und Juras 2020; Proksch et al. 2018; Bühler et al. 2017), so this is a considerable improvement. Furthermore, the assessment of snow volumes in release and deposition zones on the basis of snow depth maps and orthophotos facilitate the research on avalanche activities and characteristics of the corresponding period. Studies with UAS have already demonstrated the high importance of these measurements (Bühler et al. 2017; Eckerstorfer et al. 2016).

The crucial advantage of our procedure compared to previously performed studies with UASs is the ability to cover larger areas during periods with high avalanche activity. However, the necessity of the flight permission and the weather-dependence often prevent short-term missions.

The assessment of other hazards such as snow loading on buildings or flooding caused by rapid snow melt can also be assisted by large-scale snow depth maps. For the determination of snow loads on buildings, an adaption of our workflow would be required by using the DSM as a reference dataset and refraining from masking out settlements.

6.2.2 Planning and evaluation of avalanche protection structures and automatic weather stations

Avalanche fences and other avalanche protection structures are crucial in alpine regions for the protection of infrastructure and residents. However, the functionality of avalanche fences is only guaranteed if they are correctly placed and have a sufficient height (Margreth 2007). In our case, the snow depth map in 2019 demonstrates that the investigated wind-drift snow fences are located too closely to the release zone (Fig. 14). This increases the snow accumulation within these areas (Bühler et al. 2018a) and reduces the protective effect. Since large parts of the fences were buried by snow in 2019, the current fences may not be sufficient to prevent avalanche releases during critical periods. Accordingly, the snow depth maps can be used for large-scale evaluation of existing as well as planned avalanche protection structures (Prokop und Procter 2016). Switzerland has acknowledged the importance of snow distribution for the planning and therefore snow depth maps are established in the construction process.

Furthermore, the snow depth representativity map (Fig. 16) demonstrates how our snow depth maps can be used in models to evaluate existing AWS sites and facilitate the location identification for new AWSs which play a key role for different forecasts such as the avalanche warning service (Pérez-Guillén et al. 2022). Our snow depth maps led to the assessment of a suitable location with a high representativity for the new AWS Lukschalp (Dischma valley) which was built in 2022. Similar snow depth maps as well as the gained knowledge about snow depth distribution pattern will be applied for the planning of new AWS.

In addition, our snow depth maps enable the assessment of existing long-term AWS around Davos, which are used for various projects and avalanche forecasting. Previously, the representativity of these stations was assessed qualitatively by experts, but now, our snow depth maps enable the comparison of spatial snow depth measurements in open areas with the station measurements (Fig. 15). However, the presented results only represent the peak of winter date, accordingly, during early winter or melt season, the relation between point snow measurements to spatial snow dept distribution could be different due to changing energy balances. Further investigations are required to confirm similar snow depth distribution pattern over the entire winter season and to enable accurate interpolations from point measurement (AWS) to entire catchments.

6.2.3 Analysis of specific snow depth distribution features

Our snow depth maps play a key role in better understanding the snow depth distribution in alpine terrain. The results presented in Fig. 11 and Table 6 show the strongly varying average snow depths. and point out the added value of annual snow depth maps (Marty et al. 2019). Despite the high difference of the average snow depths, we identified a similar relative snow depth distribution (Fig. 12). Consequently, the relative snow depth distribution between different years is almost independent of the average snow depths with the exception of separate avalanche depositions zones and selected special features as they do not occur every year.

The studies of Grünewald et al. (2014) and Prokop (2008) found that snow at wind-exposed and steep areas is relocated to flatter areas and sinks. Our results confirm these observations. For example, small creeks in high-mountain catchments can be identified in our snow depth maps, because the creeks are filled with snow. Similar features can be recognised in drainage channels.

Bühler et al. (2015) and Schirmer et al. (2011) recognised the re-occurrence of cornices at the same ridges within our study area in two different years. Our data can verify the formation of this cornice in subsequent years. In addition, we determine the re-occurrence of cornices at the same locations in all of our assessed years. These cornices lead to considerably higher snow depths on the same side in each winter.

Our observations concerning the relative snow distribution correspond to the results of Schirmer et al. (2011) and Wirz et al. (2011), which found higher and lower relative snow depths on the same locations within a winter. However, all these studies were either temporally limited to only one year (Schirmer et al. 2011; Wirz et al. 2011) or the accuracy and the spatial resolution of the snow depth maps (Bühler et al. 2015; Marty et al. 2019) complicated the investigation of snow depth distribution patterns. Therefore, our snow depth maps are the first time-series which enables an extensive large-scale comparison of snow depth distribution between different years. These new possibilities lead to the confirmation of different theoretical approaches, which assume that snow depth distribution is more dependent on terrain characteristics than on the weather conditions of a certain year. This revelation opens new possibilities for the modelling of snow depths over large regions.

6.2.4 Validation dataset

Different studies have already benefited from the existing unique time-series of large snow depth maps (ADS sensor) processed by Marty et al. (2019). However, the inaccuracies and lower reliability of these snow depth maps also limited the validation and evaluation of other studies. Deep learning approaches or studies which are calibrated by exact reference data can now benefit from our improved quality. Therefore, it is to be expected that our data and approach will be used in numerous studies. For example, the snow depth maps serve as training dataset for a running project to improve the modelling of the daily snow depth distribution in Switzerland. Without our data, the model was not able to represent the snow depth distribution in complex terrain. In addition, our data could correct modelled snow depth maps which for example often exhibit a bias towards an overassessment of snow depths in high-mountain region.

Our data could also validate or evaluate numerous projects in conjunction with hydrological and snow modelling (Helbig et al. 2021; Richter et al. 2021; Vögeli et al. 2016), wind-drift models (Gerber et al. 2017; Mott et al. 2010; Schön et al. 2015), automatic detection of avalanche release zones (Bühler et al. 2018b; Bühler et al. 2022) and further snow depth models or snow depth measurements on the basis of satellite data (Leiterer et al. 2020; Wulf et al. 2020).

7 Conclusions

In this study we present the development, validation and application of a consistent and robust workflow to process aerial imagery from the state-of-the-art survey camera Vexcel Ultracam to produce reliable snow depth maps. We demonstrate its capability to capture large areas covering more than 100 km^2 under optimal as well as suboptimal acquisition conditions (varying illumination, clouds, new snow cover, absence of the NIR-band). The accuracies of our snow depth maps (RMSE: 0.15 m, Ultracam Eagle M3) are similar to results achieved with ALS and fulfil the requirements for meaningful, spatially continuous snow depth mapping in complex, open terrain. The metrics are calculated by applying an extensive accuracy assessment with check points, comparisons to UAS-derived DSMs and the evaluations of snow-free pixels, revealing a very high quality even within steep terrain. The reliability of our maps allows for the comparison of snow depth values within a 5-year period, which have shown that despite large differences of the average snow depth, the relative snow depth distribution and the formation of small-scale features is similar throughout the years.

Restrictions of the data and its acquisition are the relatively high data acquisition costs (approximately 20’000 CHF for 300 km^2) and the availability of a piloted aircraft and corresponding permissions. In addition, the procedure is limited by widespread low clouds, areas with high vegetation such as forests, the availability of accurate snow-free DTMs and powerful hardware. Even though accurate GNSS and IMU data is available from the airplane, one to five ground control points (GCPs, distribution is not important) as well as the consistent calculated masks are essential to achieve reliable results.

In particular, the high spatial resolution of our maps (0.5 m) and orthophotos (0.25 m) in conjunction with the achieved accuracy, offer the possibility to better understand the complexity of snow depth distribution in high-mountain regions. Based on the presented products, models of water stored in the snowpack (SWE) can be evaluated and improved, which is for example crucial for hydropower generation. New approaches to map snow depth with optical and radar satellites from space can be evaluated. Also, the investigation of snow avalanches benefits from such data. Several running research projects are already applying our maps for validation. We expect that in the coming years, our data will play a key role in numerous new findings in snow science.

The improvement of photogrammetry within alpine forests would be a significant step forward to equalize with the advantages of ALS. Our data allows for the extrapolation of the snow depth distribution from small areas, mapped for example by UAS, to the scale of large catchments. To further enhance the value of photogrammetric snow depth mapping, the current time series will be extended into the future. Together with datasets acquired from 2010 to 2016 with the ADS sensor within the same region, we established a unique eleven-year snow depth time series.

Data availability. The datasets used in this study will be published in ENVIDAT (https://www.envidat.ch) with the final publication of this study.

Author contributions. YB and LB designed the study. YB, AS, EH and LAE performed the fieldwork. LB processed the data with inputs from MM and YB. LB and YB prepared the manuscript with contributions from all co-authors.

Competing interests. The authors declare that they have no conflict of interest.

Acknowledgements. We would like to thank the Swiss National Science Foundation (SNF; Grant N° 200021_172800) for partly funding this project. We also thank the assistants for their help during the various fieldworks.

Financial support. This research has been partially supported by the Swiss National Science Foundation (SNF; Grant N° 200021_172800).

8 Literaturverzeichnis

Adams, Marc S.; Bühler, Yves; Fromm, Reinhard (2018): Multitemporal Accuracy and Precision Assessment of Unmanned Aerial System Photogrammetry for Slope-Scale Snow Depth Maps in Alpine Terrain. In: *Pure Appl. Geophys.* 175 (9), S. 3303–3324. DOI: 10.1007/s00024-017-1748-y.

Agisoft LLC (2020): Agisoft Metashape User Manual. Professional Edition, Version 1.6. St. Petersburg.

Avanzi, Francesco; Bianchi, Alberto; Cina, Alberto; Michele, Carlo de; Maschio, Paolo; Pagliari, Diana et al. (2018): Centimetric Accuracy in Snow Depth Using Unmanned Aerial System Photogrammetry and a MultiStation. In: *Remote Sensing* 10 (5), S. 765. DOI: 10.3390/rs10050765.

Brauchli, Tristan; Trujillo, Ernesto; Huwald, Hendrik; Lehning, Michael (2017): Influence of Slope-Scale Snowmelt on Catchment Response Simulated With the Alpine3D Model. In: *Water Resour. Res.* 53 (12), S. 10723–10739. DOI: 10.1002/2017WR021278.

Broxton, Patrick D.; van Leeuwen, Willem J. D. (2020): Structure from Motion of Multi-Angle RPAS Imagery Complements Larger-Scale Airborne Lidar Data for Cost-Effective Snow Monitoring in Mountain Forests. In: *Remote Sensing* 12 (14), S. 2311. DOI: 10.3390/rs12142311.

Brun, E.; David, P.; Sudul, M.; Brunot, G. (1992): A numerical model to simulate snow-cover stratigraphy for operational avalanche forecasting. In: *J. Glaciol.* 38 (128), S. 13–22. DOI: 10.3189/S0022143000009552.

Bühler, Y.; Bührle, L.; Eberhard, L.; Marty, M.; & Stoffel, A. (2021): Grossflächige Schneehöhen-Kartierung mit Flugzeug und Satellit. In: *Geomatik Schweiz* (119), Artikel 212 - 215.

Bühler, Y.; Eberhard, L.; Feuerstein, G.; Lurati, D.; Guler, A.; Margreth, S. (2018a): Drohneneinsatz für die Kartierung der Schneehöhenverteilung. In: *Bündnerwald* (71), S. 20–25.

Bühler, Y.; Marty, M.; Egli, L.; Veitinger, J.; Jonas, T.; Thee, P.; Ginzler, C. (2015): Snow depth mapping in high-alpine catchments using digital photogrammetry. In: *The Cryosphere* 9 (1), S. 229–243. DOI: 10.5194/tc-9-229-2015.

Bühler, Yves; Adams, Marc S.; Bösch, Ruedi; Stoffel, Andreas (2016): Mapping snow depth in alpine terrain with unmanned aerial systems (UASs): potential and limitations. In: *The Cryosphere* 10 (3), S. 1075–1088. DOI: 10.5194/tc-10-1075-2016.

Bühler, Yves; Adams, Marc S.; Stoffel, Andreas; Boesch, Ruedi (2017): Photogrammetric reconstruction of homogenous snow surfaces in alpine terrain applying near-infrared UAS imagery. In: *International Journal of Remote Sensing* 38 (8-10), S. 3135–3158. DOI: 10.1080/01431161.2016.1275060.

Bühler, Yves; Bebi, Peter; Christen, Marc; Margreth, Stefan; Stoffel, Lukas; Stoffel, Andreas et al. (2022): Automated avalanche hazard indication mapping on state wide scale.

Bühler, Yves; Hafner, Elisabeth D.; Zweifel, Benjamin; Zesiger, Mathias; Heisig, Holger (2019): Where are the avalanches? Rapid SPOT6 satellite data acquisition to map an extreme avalanche period over the Swiss Alps. In: *The Cryosphere* 13 (12), S. 3225–3238. DOI: 10.5194/tc-13-3225-2019.

Bühler, Yves; Rickenbach, Daniel von; Stoffel, Andreas; Margreth, Stefan; Stoffel, Lukas; Christen, Marc (2018b): Automated snow avalanche release area delineation – validation of existing algorithms and proposition of a new object-based approach for large-scale hazard indication mapping. In: *Nat. Hazards Earth Syst. Sci.* 18 (12), S. 3235–3251. DOI: 10.5194/nhess-18-3235-2018.

Bührle, Leon (2021): Creation, accuracy assessment and comparison of snow depth maps around Davos from Ultracam data from 2017 to 2021. Innsbruck.

Christen, M.; Kowalski, J.; Bartelt, P. (2010): RAMMS: Numerical simulation of dense snow avalanches in three-dimensional terrain. In: *Cold Regions Science and Technology* 63 (1-2), S. 1–14. DOI: 10.1016/j.coldregions.2010.04.005.

Croce, Pietro; Formichi, Paolo; Landi, Filippo; Mercogliano, Paola; Bucchignani, Edoardo; Dosio, Alessandro; Dimova, Silvia (2018): The snow load in Europe and the climate change. In: *Climate Risk Management* 20, S. 138–154. DOI: 10.1016/j.crm.2018.03.001.

Deems, Jeffrey S.; Painter, Thomas H.; Finnegan, David C. (2013): Lidar measurement of snow depth: a review. In: *J. Glaciol.* 59 (215), S. 467–479. DOI: 10.3189/2013JoG12J154.

Deschamps-Berger, César; Gascoin, Simon; Berthier, Etienne; Deems, Jeffrey; Gutmann, Ethan; Dehecq, Amaury et al. (2020): Snow depth mapping from stereo satellite imagery in mountainous terrain: evaluation using airborne laser-scanning data. In: *The Cryosphere* 14 (9), S. 2925–2940. DOI: 10.5194/tc-14-2925-2020.

Dozier, Jeff (1989): Spectral signature of alpine snow cover from the landsat thematic mapper. In: *Remote Sensing of Environment* 28, S. 9–22. DOI: 10.1016/0034-4257(89)90101-6.

Eberhard, Lucie A.; Sirguey, Pascal; Miller, Aubrey; Marty, Mauro; Schindler, Konrad; Stoffel, Andreas; Bühler, Yves (2021): Intercomparison of photogrammetric platforms for spatially continuous snow depth mapping. In: *The Cryosphere* 15 (1), S. 69–94. DOI: 10.5194/tc-15-69-2021.

Eckerstorfer, Markus; Bühler, Yves; Frauenfelder, Regula; Malnes, Eirik (2016): Remote sensing of snow avalanches: Recent advances, potential, and limitations. In: *Cold Regions Science and Technology* 121, S. 126–140. DOI: 10.1016/j.coldregions.2015.11.001.

Eckerstorfer, Markus; Vickers, Hannah; Malnes, Eirik; Grahn, Jakob (2019): Near-Real Time Automatic Snow Avalanche Activity Monitoring System Using Sentinel-1 SAR Data in Norway. In: *Remote Sensing* 11 (23), S. 2863. DOI: 10.3390/rs11232863.

Eker, Remzi; Bühler, Yves; Schlögl, Sebastian; Stoffel, Andreas; Aydın, Abdurrahim (2019): Monitoring of Snow Cover Ablation Using Very High Spatial Resolution Remote Sensing Datasets. In: *Remote Sensing* 11 (6), S. 699. DOI: 10.3390/rs11060699.

Essery, R. (2015): A factorial snowpack model (FSM 1.0). In: *Geosci. Model Dev.* 8 (12), S. 3867–3876. DOI: 10.5194/gmd-8-3867-2015.

Federal Office of Topography swisstopo (2021a): 02.11.2021.
https://www.swisstopo.admin.ch/en/geodata/landscape/tlm3d.html, zuletzt geprüft am 03.11.2021.

Feistl, T.; Bebi, P.; Dreier, L.; Hanewinkel, M.; Bartelt, P. (2014): Quantification of basal friction for technical and silvicultural glide-snow avalanche mitigation measures. In: *Nat. Hazards Earth Syst. Sci.* 14 (11), S. 2921–2931. DOI: 10.5194/nhess-14-2921-2014.

Gerber, F.; Lehning, M.; Hoch, S. W.; Mott, R. (2017): A close-ridge small-scale atmospheric flow field and its influence on snow accumulation. In: *J. Geophys. Res. Atmos.* 122 (15), S. 7737–7754. DOI: 10.1002/2016JD026258.

Gerber, Franziska; Mott, Rebecca; Lehning, Michael (2019): The Importance of Near-Surface Winter Precipitation Processes in Complex Alpine Terrain. In: *Journal of Hydrometeorology* 20 (2), S. 177–196. DOI: 10.1175/JHM-D-18-0055.1.

Gindraux, Saskia; Boesch, Ruedi; Farinotti, Daniel (2017): Accuracy Assessment of Digital Surface Models from Unmanned Aerial Vehicles' Imagery on Glaciers. In: *Remote Sensing* 9 (2), S. 186. DOI: 10.3390/rs9020186.

GLAMOS - Glacier Monitoring Switzerland (2021): Swiss Glacier Mass Balance 2020 (release 2021). Unter Mitarbeit von Matthias Huss, Andreas Bauder, Mauro Fischer, Martin Funk, Giovanni Kappenberger, Andreas Linsbauer et al.

Griessinger, Nena; Mohr, Franziska; Jonas, Tobias (2018): Measuring snow ablation rates in alpine terrain with a mobile multioffset ground-penetrating radar system. In: *Hydrol. Process.* DOI: 10.1002/hyp.13259.

Grünewald, T.; Bühler, Y.; Lehning, M. (2014): Elevation dependency of mountain snow depth. In: *The Cryosphere* 8 (6), S. 2381–2394. DOI: 10.5194/tc-8-2381-2014.

Grünewald, T.; Schirmer, M.; Mott, R.; Lehning, M. (2010): Spatial and temporal variability of snow depth and ablation rates in a small mountain catchment. In: *The Cryosphere* 4 (2), S. 215–225. DOI: 10.5194/tc-4-215-2010.

Hafner, Elisabeth D.; Techel, Frank; Leinss, Silvan; Bühler, Yves (2021): Mapping avalanches with satellites – evaluation of performance and completeness. In: *The Cryosphere* 15 (2), S. 983–1004. DOI: 10.5194/tc-15-983-2021.

Hall, Dorothy K.; Riggs, George A.; Salomonson, Vincent V. (1995): Development of methods for mapping global snow cover using moderate resolution imaging spectroradiometer data. In: *Remote Sensing of Environment* 54 (2), S. 127–140. DOI: 10.1016/0034-4257(95)00137-P.

Harder, Phillip; Pomeroy, John W.; Helgason, Warren D. (2020): Improving sub-canopy snow depth mapping with unmanned aerial vehicles: lidar versus structure-from-motion techniques. In: *The Cryosphere* 14 (6), S. 1919–1935. DOI: 10.5194/tc-14-1919-2020.

Harder, Phillip; Schirmer, Michael; Pomeroy, John; Helgason, Warren (2016): Accuracy of snow depth estimation in mountain and prairie environments by an unmanned aerial vehicle. In: *The Cryosphere* 10 (6), S. 2559–2571. DOI: 10.5194/tc-10-2559-2016.

Helbig, Nora; Bühler, Yves; Eberhard, Lucie; Deschamps-Berger, César; Gascoin, Simon; Dumont, Marie et al. (2021): Fractional snow-covered area: scale-independent peak of winter parameterization. In: *The Cryosphere* 15 (2), S. 615–632. DOI: 10.5194/tc-15-615-2021.

Helfricht, K.; Kuhn, M.; Keuschnig, M.; Heilig, A. (2014): Lidar snow cover studies on glaciers in the Ötztal Alps (Austria): comparison with snow depths calculated from GPR measurements. In: *The Cryosphere* 8 (1), S. 41–57. DOI: 10.5194/tc-8-41-2014.

Höhle, Joachim; Höhle, Michael (2009): Accuracy assessment of digital elevation models by means of robust statistical methods. In: *ISPRS Journal of Photogrammetry and Remote Sensing* 64 (4), S. 398–406. DOI: 10.1016/j.isprsjprs.2009.02.003.

Jacobs, Jennifer M.; Hunsaker, Adam G.; Sullivan, Franklin B.; Palace, Michael; Burakowski, Elizabeth A.; Herrick, Christina; Cho, Eunsang (2021): Snow depth mapping with unpiloted aerial system lidar observations: a case study in Durham, New Hampshire, United States. In: *The Cryosphere* 15 (3), S. 1485–1500. DOI: 10.5194/tc-15-1485-2021.

Koenderink, J. J.; van Doorn, A. J. (1991): Affine structure from motion. In: *Journal of the Optical Society of America. A, Optics and image science* 8 (2), S. 377–385. DOI: 10.1364/JOSAA.8.000377.

Korzeniowska, Karolina; Bühler, Yves; Marty, Mauro; Korup, Oliver (2017): Regional snow-avalanche detection using object-based image analysis of near-infrared aerial imagery. In: *Nat. Hazards Earth Syst. Sci.* 17 (10), S. 1823–1836. DOI: 10.5194/nhess-17-1823-2017.

Kulakowski, Dominik; Bebi, Peter; Rixen, Christian (2011): The interacting effects of land use change, climate change and suppression of natural disturbances on landscape forest structure in the Swiss Alps. In: *Oikos* 120 (2), S. 216–225. DOI: 10.1111/j.1600-0706.2010.18726.x.

Leinss, Silvan; Wicki, Raphael; Holenstein, Sämi; Baffelli, Simone; Bühler, Yves (2020): Snow avalanche detection and mapping in multitemporal and multiorbital radar images from TerraSAR-X and Sentinel-1. In: *Nat. Hazards Earth Syst. Sci.* 20 (6), S. 1783–1803. DOI: 10.5194/nhess-20-1783-2020.

Leiterer, Reik; Wulf, Hendri; Milani, Gillian; Sassik, Bernhard; Bühler, Yves; Wegner, Jan (2020): Schneekartierung aus dem All – das Potenzial frei verfügbarer Satellitendaten. In: *«Wasser Energie Luft* (3), S. 171–174.

Linsbauer, Andreas; Huss, Matthias; Hodel, Elias; Bauder, Andreas; Fischer, Mauro; Weidmann, Yvo et al. (2021): The New Swiss Glacier Inventory SGI2016: From a Topographical to a Glaciological Dataset. In: *Front. Earth Sci.* 9, Artikel 704189. DOI: 10.3389/feart.2021.704189.

López-Moreno, Juan I.; Revuelto, Jesús; Alonso-González, E.; Sanmiguel-Vallelado, Alba; Fassnacht, Steven R.; Deems, Jeffrey; Morán-Tejeda, Enrique (2017): Using very long-range terrestrial laser scanner to analyze the temporal consistency of the snowpack distribution in a high mountain environment. In: *J. Mt. Sci.* 14 (5), S. 823–842. DOI: 10.1007/s11629-016-4086-0.

Lowe, David G. (2004): Distinctive Image Features from Scale-Invariant Keypoints. In: *International Journal of Computer Vision* 60 (2), S. 91–110. DOI: 10.1023/B:VISI.0000029664.99615.94.

Magnusson, Jan; Nævdal, Geir; Matt, Felix; Burkhart, John F.; Winstral, Adam (2020): Improving hydropower inflow forecasts by assimilating snow data. In: *Hydrology Research* 51 (2), S. 226–237. DOI: 10.2166/nh.2020.025.

Margreth, Stefan (2007): Defense structures in avalanche starting zones. Technical guideline as an aid to enforcement.

Marti, R.; Gascoin, S.; Berthier, E.; Pinel, M. de; Houet, T.; Laffly, D. (2016): Mapping snow depth in open alpine terrain from stereo satellite imagery. In: *The Cryosphere* 10 (4), S. 1361–1380. DOI: 10.5194/tc-10-1361-2016.

Marty, M.; Bühler, Y.; Ginzler, C. (2019): Snow Depth Mapping. Unter Mitarbeit von Mauro Marty.

Mazzotti, Giulia; Currier, William Ryan; Deems, Jeffrey S.; Pflug, Justin M.; Lundquist, Jessica D.; Jonas, Tobias (2019): Revisiting Snow Cover Variability and Canopy Structure Within Forest Stands: Insights From Airborne Lidar Data. In: *Water Resour. Res.* 55 (7), S. 6198–6216. DOI: 10.1029/2019WR024898.

McGrath, Daniel; Webb, Ryan; Shean, David; Bonnell, Randall; Marshall, Hans-Peter; Painter, Thomas H. et al. (2019): Spatially Extensive Ground-Penetrating Radar Snow Depth Observations During NASA's 2017 SnowEx Campaign: Comparison With In Situ, Airborne, and Satellite Observations. In: *Water Resour. Res.* 55 (11), S. 10026–10036. DOI: 10.1029/2019WR024907.

Meyer, Joachim; Deems, Jeffrey S.; Bormann, Kat J.; Shean, David E.; Skiles, S. McKenzie (2022): Mapping snow depth and volume at the alpine watershed scale from aerial imagery using Structure from Motion. In: *Front. Earth Sci.* 10, Artikel 989792. DOI: 10.3389/feart.2022.989792.

Meyer, Joachim; Skiles, S. McKenzie (2019): Assessing the Ability of Structure From Motion to Map High-Resolution Snow Surface Elevations in Complex Terrain: A Case Study From Senator Beck Basin, CO. In: *Water Resour. Res.* 55 (8), S. 6596–6605. DOI: 10.1029/2018WR024518.

Michele, Carlo de; Avanzi, Francesco; Passoni, Daniele; Barzaghi, Riccardo; Pinto, Livio; Dosso, Paolo et al. (2016): Using a fixed-wing UAS to map snow depth distribution: an evaluation at peak accumulation. In: *The Cryosphere* 10 (2), S. 511–522. DOI: 10.5194/tc-10-511-2016.

Mietkiewicz, Nathan; Kulakowski, Dominik; Rogan, John; Bebi, Peter (2017): Long-term change in sub-alpine forest cover, tree line and species composition in the Swiss Alps. In: *J Veg Sci* 28 (5), S. 951–964. DOI: 10.1111/jvs.12561.

Miller, Zachary S.; Peitzsch, Erich H.; Sproles, Eric A.; Birkeland, Karl W.; Palomaki, Ross T. (2022): Assessing the seasonal evolution of snow depth spatial variability and scaling in complex mountain terrain. In: *The Cryosphere* 16 (12), S. 4907–4930. DOI: 10.5194/tc-16-4907-2022.

Mott, R.; Schirmer, M.; Bavay, M.; Grünewald, T.; Lehning, M. (2010): Understanding snow-transport processes shaping the mountain snow-cover. In: *The Cryosphere* 4 (4), S. 545–559. DOI: 10.5194/tc-4-545-2010.

Nolan, M.; Larsen, C.; Sturm, M. (2015): Mapping snow depth from manned aircraft on landscape scales at centimeter resolution using structure-from-motion photogrammetry. In: *The Cryosphere* 9 (4), S. 1445–1463. DOI: 10.5194/tc-9-1445-2015.

Painter, Thomas H.; Berisford, Daniel F.; Boardman, Joseph W.; Bormann, Kathryn J.; Deems, Jeffrey S.; Gehrke, Frank et al. (2016): The Airborne Snow Observatory: Fusion of scanning lidar, imaging spectrometer, and physically-based modeling for mapping snow water equivalent and snow albedo. In: *Remote Sensing of Environment* 184, S. 139–152. DOI: 10.1016/j.rse.2016.06.018.

Pérez-Guillén, Cristina; Techel, Frank; Hendrick, Martin; Volpi, Michele; van Herwijnen, Alec; Olevski, Tasko et al. (2022): Data-driven automated predictions of the avalanche danger level for dry-snow conditions in Switzerland. In: *Nat. Hazards Earth Syst. Sci.* 22 (6), S. 2031–2056. DOI: 10.5194/nhess-22-2031-2022.

Prokop, Alexander (2008): Assessing the applicability of terrestrial laser scanning for spatial snow depth measurements. In: *Cold Regions Science and Technology* 54 (3), S. 155–163. DOI: 10.1016/j.coldregions.2008.07.002.

Prokop, Alexander; Procter, Emily S. (2016): A new methodology for planning snow drift fences in alpine terrain. In: *Cold Regions Science and Technology* 132, S. 33–43. DOI: 10.1016/j.coldregions.2016.09.010.

Proksch, Martin; Dräyer, Bernhard; Pašić, Ivan; Burkard, André; Carlen, Norbert (2018): The valalanche project: Putting recent progress in snow avalanche mapping into practice. In: *International Snow Science Workshop*, S. 826–829.

Revuelto, Jesús; Alonso-Gonzalez, Esteban; Vidaller-Gayan, Ixeia; Lacroix, Emilien; Izagirre, Eñaut; Rodríguez-López, Guillermo; López-Moreno, Juan Ignacio (2021): Intercomparison of UAV platforms for mapping snow depth distribution in complex alpine terrain. In: *Cold Regions Science and Technology* 190, S. 103344. DOI: 10.1016/j.coldregions.2021.103344.

Richter, Bettina; Schweizer, Jürg; Rotach, Mathias W.; van Herwijnen, Alec (2021): Modeling spatially distributed snow instability at a regional scale using Alpine3D. In: *J. Glaciol.*, S. 1–16. DOI: 10.1017/jog.2021.61.

Sanz-Ablanedo, Enoc; Chandler, Jim; Rodríguez-Pérez, José; Ordóñez, Celestino (2018): Accuracy of Unmanned Aerial Vehicle (UAV) and SfM Photogrammetry Survey as a Function of the Number and Location of Ground Control Points Used. In: *Remote Sensing* 10 (10), S. 1606. DOI: 10.3390/rs10101606.

Schirmer, M.; Wirz, V.; Clifton, A.; Lehning, M. (2011): Persistence in intra-annual snow depth distribution: 1. Measurements and topographic control. In: *Water Resour. Res.* 47 (9). DOI: 10.1029/2010WR009426.

Schlögl, Sebastian; Lehning, Michael; Fierz, Charles; Mott, Rebecca (2018): Representation of Horizontal Transport Processes in Snowmelt Modeling by Applying a Footprint Approach. In: *Front. Earth Sci.* 6, Artikel 120. DOI: 10.3389/feart.2018.00120.

Schneider, S.; Gruber, M. (2008): RADIOMETRIC QUALITY OF ULTRACAM-X IMAGES. In: *The International Archives of the Photogrammetry, Remote Sensing and Spatial Information Sciences* (37), S. 539–544.

Schön, Peter; Prokop, Alexander; Vionnet, Vincent; Guyomarc'h, Gilbert; Naaim-Bouvet, Florence; Heiser, Micha (2015): Improving a terrain-based parameter for the assessment of snow depths with TLS data in the Col du Lac Blanc area. In: *Cold Regions Science and Technology* 114, S. 15–26. DOI: 10.1016/j.coldregions.2015.02.005.

Shaw, Thomas E.; Gascoin, Simon; Mendoza, Pablo A.; Pellicciotti, Francesca; McPhee, James (2020): Snow Depth Patterns in a High Mountain Andean Catchment from Satellite Optical Tristereoscopic Remote Sensing. In: *Water Resour. Res.* 56 (2). DOI: 10.1029/2019WR024880.

Souckova, Marketa; Juras, Roman (2020): Mapping snow avalanche releases by unmanned aerial vehicles (UAV) in Krkonoše mountain range, the Czech Republic.

Spandre, Pierre; François, Hugues; Thibert, Emmanuel; Morin, Samuel; George-Marcelpoil, Emmanuelle (2017): Determination of snowmaking efficiency on a ski slope from observations and modelling of snowmaking events and seasonal snow accumulation. In: *The Cryosphere* 11 (2), S. 891–909. DOI: 10.5194/tc-11-891-2017.

Triggs, Bill; McLauchlan, Philip F.; Hartley, Richard I.; Fitzgibbon, Andrew W. (2000): Bundle Adjustment — A Modern Synthesis. In: Gerhard Goos, Juris Hartmanis, Jan van Leeuwen, Bill Triggs, Andrew Zisserman und Richard Szeliski (Hg.): Vision Algorithms: Theory and Practice, Bd. 1883. Berlin, Heidelberg: Springer Berlin Heidelberg (Lecture Notes in Computer Science), S. 298–372.

Vögeli, Christian; Lehning, Michael; Wever, Nander; Bavay, Mathias (2016): Scaling Precipitation Input to Spatially Distributed Hydrological Models by Measured Snow Distribution. In: *Front. Earth Sci.* 4. DOI: 10.3389/feart.2016.00108.

Westoby, M. J.; Brasington, J.; Glasser, N. F.; Hambrey, M. J.; Reynolds, J. M. (2012): 'Structure-from-Motion' photogrammetry: A low-cost, effective tool for geoscience applications. In: *Geomorphology* 179, S. 300–314. DOI: 10.1016/j.geomorph.2012.08.021.

Wipf, Sonja; Stoeckli, Veronika; Bebi, Peter (2009): Winter climate change in alpine tundra: plant responses to changes in snow depth and snowmelt timing. In: *Climatic Change* 94 (1-2), S. 105–121. DOI: 10.1007/s10584-009-9546-x.

Wirz, V.; Schirmer, M.; Gruber, S.; Lehning, M. (2011): Spatio-temporal measurements and analysis of snow depth in a rock face. In: *The Cryosphere* 5 (4), S. 893–905. DOI: 10.5194/tc-5-893-2011.

Wulf, Hendrik; Sassik, Bernhard; Milani, Gillian; Leiterer, Reik (2020): High-resolution snow depth monitoring for entire mountain ranges. In: 2020 7th Swiss Conference on Data Science (SDS). 2020 7th Swiss Conference on Data Science (SDS). Luzern, Switzerland, 26.06.2020 - 26.06.2020: IEEE, S. 1–4.

9 Appendix

Appendix A. Overview reference points in 2020

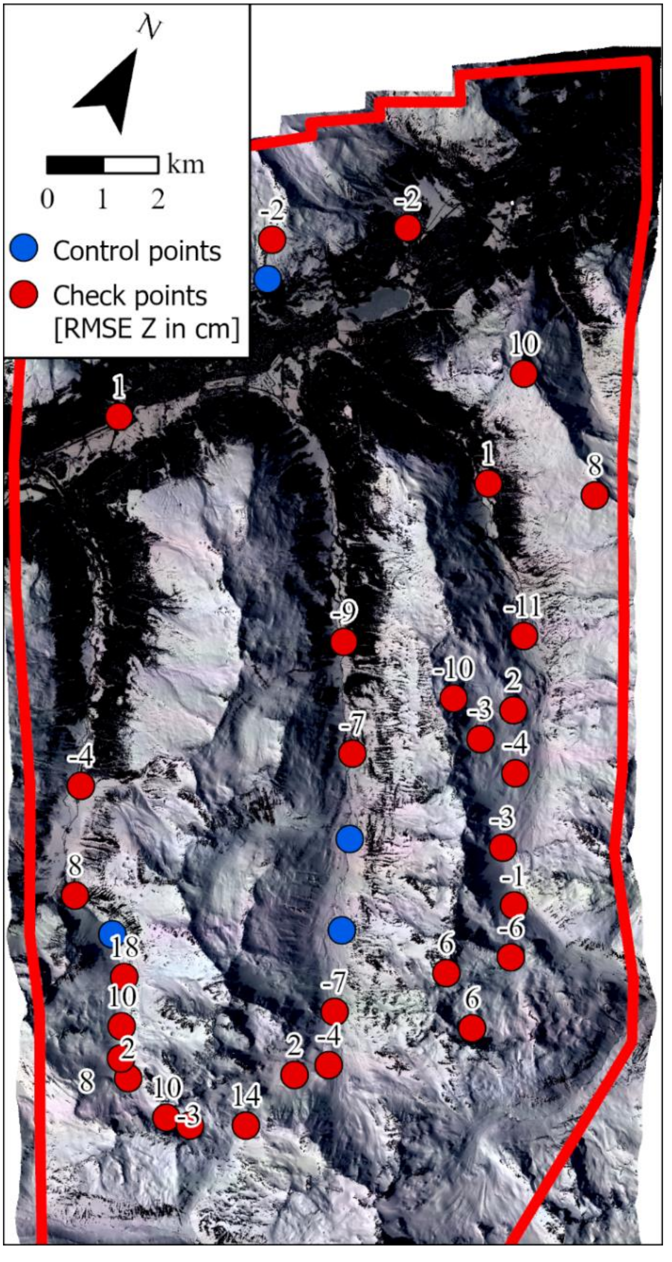

Figure A1. Overview of the distribution of ground control points (red) and check points (blue) with the corresponding RMSE Z values. Background shows the orthophoto from 2020.

Appendix B. Overview area and percentage of masks used.

Table A2. Area [km²] and percentage [%] of various masks, outliers and remaining snow depth values for all snow depth maps.

Year		Water	Glacier	Building & infrastructure	High vegetation	Outlier	Snow depth values
2017	Area [km²]	2.2	3.4	13.3	221.3	19.2	369.8
	Percentage [%]	0.3	0.5	2.1	35.2	3.0	58.8
2018	Area [km²]	0.3	0.0	4.5	30.7	0.2	35.6
	Percentage [%]	0.5	0.0	6.2	43.1	0.3	50.1
2019	Area [km²]	1.1	2.7	6.7	61.8	1.1	167.4
	Percentage [%]	0.5	1.1	2.7	25.7	0.5	69.7
2020	Area [km²]	1.1	2.7	6.6	60.6	1.7	161.3
	Percentage [%]	0.5	1.2	2.7	25.9	0.7	69.0
2021	Area [km²]	1.1	2.7	6.8	58.2	2.2	149.4
	Percentage [%]	0.5	1.2	3.0	26.4	1.0	67.9